$(e, e'p)$ Studies of the Deuteron at High Q^2

(Experiment E-01-020)

M. Epstein
The California State University at Los Angeles

J.-M. Laget
Centre d'Etudes de Saclay, Gif-sur-Yvette

J.M. Finn, C. Perdrisat
The College of William and Mary

W. Boeglin *(cospokesperson)*, F. Klein, L. Kramer, P.E.C. Markowitz, B. Raue, J. Reinhold, M. Sargsian
Florida International University

S. Strauch
George Washington University

G. Batigne, C. Furget, S. Kox, E. Liatard, J. Mougey, E. Penel, J.-S. Réal, R. Tieulent, E. Voutier *(cospokesperson)*
Institut des Sciences Nucléaires, Grenoble

K. de Jager, R. Ent, D.W. Higinbotham, M. Jones *(cospokesperson)* J. LeRose, A. Saha
Jefferson Laboratory

K. McCormick
Kent State University

W. Bertozzi, S. Gilad, M. Rvachev, S. Sirca, R. Suleiman, Z. Zhou
Massachusetts Institute of Technology

V. Punjabi
Norfolk State University

J. Adam
Nuclear Physics Institute, Rez n. Prague, Czech Republic

S. Jeschonnek
Ohio State University

C.E. Hyde-Wright, H. Ibrahim, A. Klein *(cospokesperson)*, S. Kuhn, P.E. Ulmer *(contact person, cospokesperson)*, L.B. Weinstein
Old Dominion University

M. Strikman
Pennsylvania State University

J. Mitchell
Renaissance Technologies

F. Benmokhtar, S. Dieterich, R. Gilman, X. Jiang, R.D. Ransome
Rutgers University

A. Sarty
St. Mary's University

E. Piasetzky
Tel Aviv University

J. Templon
The University of Georgia

Z. Papandreou
The University of Regina

Contents

1 Overview

To comply with the PAC's requirement, proposals PR-01-007 and PR-01-008 have been merged into this single document (experiment E-01-020). This required establishing a common set of kinematics where we selected Q^2 values intermediate between those of the original proposals. These relatively minor adjustments will not compromise the physics goals in any way. Moreover, the overall beam time was reduced somewhat due to the slightly lower Q^2 values compared to proposal PR-01-008. Due to this savings and the degree of overlap between the original proposals, we will be able to achieve the physics goals of both proposals in the allotted time of 30 days. (As the motivations have not changed and for the sake of completeness, the motivation sections from PR-01-007 and PR-01-008 are simply repeated here.)

All measurements are now carried out at constant values of Q^2 and for the same range of recoil momenta. As before the angular distributions will be measured for the recoil momenta of $p_{miss} = 0.2, 0.4$ and 0.5 GeV/c. The R_{LT} response functions will be determined for recoil momenta $p_{miss} = 0., 0.1, 0.2, 0.3, 0.4$ and 0.5 GeV/c. The R_{LT} measurements also provide part of the data for the angular distributions.

Detailed kinematics are given in the subsequent sections. Although the Q^2 values are somewhat higher than those of PR-01-007, the higher beam energies assumed (4.7 GeV for the two higher Q^2 values compared to 4.0 GeV in PR-01-007) more than compensate, giving an overall higher coincidence event rate. Further, the constraint of fixing the electron angle for the PR-01-007 parallel/anti-parallel kinematics measurements was removed, so that this scan is now done at constant Q^2, as required by PR-01-008. This too, does not compromise any of the physics goals (the former choice was driven only by considerations of minimizing the overhead).

2 Physics Motivation: R_{LT} and p_{miss} Dependence

2.1 Importance of the Deuteron

The deuteron, as the only bound two-nucleon system represents the simplest manifestation of the nuclear force. It therefore provides a benchmark in nuclear physics for one cannot hope to understand complex nuclei without first understanding the deuteron.

Although the deuteron is a loosely bound system its high momentum structure is strikingly similar to that of more complex nuclei [1]. Thus, measurement of high momentum components of the deuteron wave function can guide our understanding of the correlation structure of complex nuclei. Beyond about 0.3 GeV/c recoil momentum, the D-state component of the wave function is emphasized. A precise measurement in this range would provide important constraints for nucleon-nucleon potentials. It should be stressed, however, that the momentum distribution is not an observable and can only be extracted in the context of a model. For example, final state interactions can significantly alter the momentum of the detected nucleon and therefore the inferred initial momentum. Studies of the deuteron will also help to pin down these effects (see below) so that more quantitative statements about the deuteron wave function can be made. This information is important input for the understanding of the structure of more complex nuclei.

An example is the recently approved Hall A proposal to measure the $^{16}\mathrm{O}(e,e'p)$ reaction [2] which is an update of an earlier Hall A measurement. The most modern relativistic Distorted Wave Impulse Approximation (DWIA) calculations were quite successful in reproducing the p-shell data from this earlier experiment and also showed evidence of dynamical relativistic effects in the left-right asymmetry (related to R_{LT}) [3]. The new $^{16}\mathrm{O}$ proposal plans to push the kinematics to higher recoil momenta to test whether or where the single-particle DWIA model breaks down. Our $^2\mathrm{H}(e,e'p)n$ proposal also involves measurements of R_{LT} (and hence the left-right asymmetry) over a range of Q^2 and p_r to test the validity of various relativistic treatments. As the deuteron is a simpler system, it provides a natural starting point for testing such models. The information gleaned from our experiment will be a critical component to interpreting this other experiment.

Coincidence $^2\mathrm{H}(e,e'p)n$ reactions are particularly well suited to NN interaction studies. Below pion threshold, the final state is completely specified. For example, Fabian and Arenhövel have performed a nonrelativistic treatment of deuteron electrodistintegration in $(e,e'p)$ in which they examined the importance of interaction effects (Meson Exchange Currents (MEC) and Isobar Configurations (IC)) over the kinematical phase space below pion threshold [4]. Off the quasielastic peak they predict large changes in the cross section (reflecting mostly the transverse response, R_T) due to the presence of these interaction effects. In particular, at low momentum transfers and high np relative energies, they expect large modifications from ICs. Conversely, at high momentum transfers and low np relative energies, they expect large modifications from MECs. Therefore, by performing systematic studies over a broad kinematical range, the role played by various interaction effects can be quantified. Further, at large values of Q^2, relativistic effects should be important. In fact, data at relatively low Q^2 from NIKHEF already indicate the need for a relativistic treatment in order to properly describe the R_{LT} response function [5] [6].

The deuteron is a valuable tool not only for what it can tell us about the nuclear force but also as a source of neutrons. Lacking pure neutron targets, the deuteron with its relatively loose binding is often chosen for studies of the structure of the neutron. Measurements of elastic electron scattering from deuterium have been used extensively

in order to extract the long sought after and poorly known neutron electric form factor, G_{En}. There is also considerable interest in $^2\mathrm{H}(\vec{e}, e'\vec{n})p$ polarization transfer measurements since various calculations predict that at small recoil momentum the observable of interest is sensitive to G_{En} [7] but relatively insensitive to NN interaction effects and to the deuteron wavefunction [8]. All of the above neutron studies rely on the assumption that nuclear corrections for the deuteron are either small or well understood. It is therefore vitally important to these measurements that this assumption be thoroughly tested. Understanding the deuteron is also important for measurements employing deuterium targets to determine the spin structure function of the neutron.

Finally, by studying the very short distance structure of the deuteron, one may determine whether or to what extent the description of nuclei in terms of nucleon/meson degrees of freedom must be supplemented by inclusion of explicit quark effects. This issue is of fundamental importance to nuclear physics.

2.2 Overview of Existing Data on $^2\mathrm{H}(e, e'p)n$

The large body of data on the $^2\mathrm{H}(e, e'p)n$ reaction serves as further testament to the importance of this reaction in nuclear physics. However, only with JLAB's unique combination of energy, current, duty factor and control of systematics (achievable in Hall A) can a truly systematic study be undertaken. This is especially true if one wishes to understand the short-distance structure of the deuteron where one needs both high energies and high luminosity/duty factor.

The short range structure of the deuteron is best revealed by measuring very high recoil momenta in $^2\mathrm{H}(e, e'p)n$. Further, separations of the cross section into the various response functions allow one to exploit the sensitivity inherent in various interferences of components of the nuclear current. There is a substantial body of data on this reaction, including unseparated cross sections [9, 10, 11, 12] as well as separations of the various response functions [5, 13, 14, 15, 16, 17, 18, 19, 20]. Further, several experiments involving measurement of the ejected proton polarization have been carried out at Bates [21, 22, 23].

For the cross section measurements, limitations in energy of the various facilities (Bates/Saclay/NIKHEF/Mainz) have frustrated attempts to access the short distance structure of the deuteron [10, 12]. This limitation necessarily forces measurement of very high recoil momenta to energy transfers far above the quasielastic peak. Thus, for the Turck-Chieze and high recoil Blomqvist data, the kinematics were in the delta-region where lack of knowledge of the reaction mechanism make it difficult to deduce aspects of the deuteron structure. Although this limitation is not shared by SLAC, limitations in current and duty factor restrict the range of recoil momenta there as well. Although the Mainz [12] measurement sampled recoils up to 928 MeV/c, the kinematics actually imply that the bulk of the cross section arises from interaction with the neutron, leaving the detected proton as a spectator. Within this proton spectator picture, the actual internal momentum probed in this process is not the recoil momentum, but the momentum of the detected proton ($\sim$ 670 MeV/c). Further, since the kinematics were in the delta-region of the inclusive (e, e') spectrum, the inclusion of virtual nucleon excitations was required to obtain agreement with the data. In contrast, at JLAB one can examine large recoil momenta at or even below quasifree kinematics, making the extraction of the deuteron structure less model-dependent. It is stressed that **JLAB is the only facility in the world where such a study can be undertaken.** This experiment would exploit this

unique opportunity.

The d$(e, e'p)$n separation experiments have revealed gaps in our understanding. Various calculations have difficulty reproducing both R_L and R_T [14, 16, 18]. The R_{LT} response and related A_ϕ asymmetry indicate the need for relativistic treatments [5, 15, 16, 17] but problems still exist in reproducing the data. Again, JLAB provides the kinematic flexibility to perform these separations over a broad range of recoil momenta and momentum transfers. Here, we focus on a separation of R_{LT} as it is less technically demanding than separations of R_L and R_T.

2.3 Motivation for Parallel/Anti-Parallel Kinematics

In order to unravel the deuteron short-distance structure, one must either select kinematics which minimize reaction effects or correctly account for such effects. One of the main obstructions is FSI since they can change the cross section at high recoil momenta by an order of magnitude or more. These large effects result from strength at low initial proton momentum, p_i, appearing at higher inferred p_i due to np rescattering in the final state. Such effects are likely to be large in perpendicular kinematics, but can be substantially reduced in parallel/anti-parallel kinematics. A simple picture illustrates this and is shown in Figure 1. Here, it's assumed that the rescattering mostly results in a change of the proton angle and not its energy. In this case, rescattering can lead to a larger inferred initial momentum for perpendicular kinematics, whereas for parallel or anti-parallel kinematics, rescattering can only produce a smaller initial momentum. Thus, within this highly oversimplified picture, for the parallel and anti-parallel cases one does not get feeding from smaller initial momentum, in contrast to the case for perpendicular kinematics. Naturally, one needs to go beyond this and perform a real calculation. The results of Arenhövel's calculation are shown in Table 1 for the middle Q^2 kinematics of this proposal. Here, "FSI/PWBA" refers to his calculation including FSI effects compared to the one without (Plane Wave Born Approximation). It is seen that rescattering gives an enhancement factor of 14 for the highest recoil momentum measured, compared to only 2.5 for the anti-parallel kinematics case. **The conclusion: the high recoil momentum spectrum in parallel/anti-parallel kinematics is much more connected to the deuteron short-distance structure than in perpendicular kinematics.**

For the "anti-parallel" kinematics measurements (*i.e.* the ones below the quasifree peak), the momentum transfer was chosen to be sufficiently large in order to avoid significant contribution of the "spectator diagram" where the neutron is struck and the spectator proton is detected. Figure 2 illustrates this. In the left panel, the proton, initially moving opposite to $\vec{q}$ absorbs the momentum transfer leading to the final state shown (the neutron, as a spectator, simply keeps the momentum it had initially). The right panel shows the situation where the neutron receives $\vec{q}$ and the proton is a spectator. For the situation shown, the proton spectator diagram corresponds to low proton initial momentum, $\vec{p}_i$, but high recoil momentum, $\vec{p}_r$ ($\vec{p}_r$ is the just the neutron final state momentum). High $\vec{p}_r$ does not, therefore, necessarily correspond to high internal (*i.e.* initial) proton momentum, and, in fact, the proton spectator diagram would dominate the cross section in this case. However, if one selects a momentum transfer more than twice the largest recoil momentum, this situation cannot arise since the proton spectator diagram will involve an initial momentum larger than that for the neutron spectator diagram. Thus, for our anti-parallel kinematics, we have chosen a momentum transfer which is more than twice as large as the highest recoil momentum sampled. The anti-parallel kinematics then

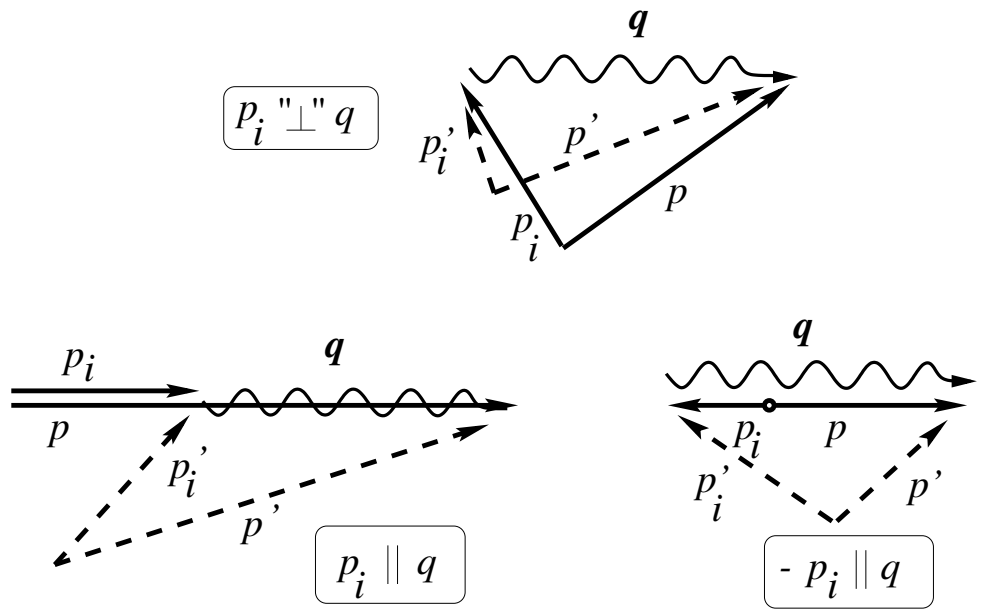

Figure 1: Rescattering cartoons. The measured values of the proton momentum (p) and momentum transfer (q) are shown by the solid arrows. The inferred value of the proton initial momentum is then p_i. However, the measured value of p can arise from a "true" value, p' (dashed arrow) which then changes to p by rescattering. The actual value of the initial momentum is then p_i' (dashed arrow). The situation is shown for "perpendicular", parallel and anti-parallel kinematics. (Perpendicular kinematics refers to the case where the initial momentum and $\vec{q}$ are roughly at right angles. More precisely, it corresponds to fixed $\vec{q}$ and ω.) The perpendicular kinematic case is shown only for the undesirable situation where low initial momentum feeds high recoil momentum (the reverse is also possible).

p_r MeV/c	FSI/PWBA $\perp$ Kin	FSI/PWBA Anti-$\parallel$ Kin
160	0.7	0.9
270	1.2	0.9
440	8.0	1.4
600	14	2.5

Table 1: Comparison of effects of FSI for perpendicular kinematics *vs.* anti-parallel kinematics for the middle Q^2 kinematics. The column labeled "FSI/PWBA" is the ratio of Arenhövel's calculation including FSI to his PWBA calculation. The comparison is made for $\phi_x = 0^\circ$ in perpendicular kinematics and for $x > 1$ in anti-parallel kinematics. The ratios are given for roughly comparable recoil momenta (first column) for the two measurements.

corresponds to the virtual photon essentially reversing the direction of the struck proton (see Figure 3). The point at which the proton's initial momentum is equal to $\vec{q}/2$ would then correspond to a final state where the neutron and proton are moving in the same direction with equal momentum. This corresponds to threshold electro-disintegration. To avoid this kinematics and the relatively large FSI which would result, $\vec{q}$ had to be chosen somewhat above twice the highest sampled recoil momentum.

Due to the lower bound on Q^2 from the above arguments and due to the fact that at even higher Q^2, calculations of FSI, *etc.* become more unreliable and counting rates become more problematic, the measurements in parallel/anti-parallel kinematics will focus on the middle Q^2 value. They will span values of x above and below the quasifree peak for fixed beam energy and electron scattering angle. Although FSI are expected to be relatively smaller for parallel/anti-parallel kinematics, one must still account for these and other reaction effects. The precision of the data gathered here would be adequate to clearly quantify the importance of these effects. This is illustrated in Figures 4 and 5 which show calculations of the cross section by Arenhövel [24] for a sample of the kinematics which would be measured. (The labeling of the various panels corresponds with the kinematics tables given below. "PY_4" and "PY_2" correspond to $+y$, *i.e.* energy transfers above the quasifree peak. "q2_00" is for $y = 0$ (*i.e.* on top of the quasifree peak or at $x = 1$; this point is the same as the zero recoil momentum point of the middle Q^2 perpendicular kinematics measurement). Finally "NY_2" and "NY_4" correspond to $-y$, *i.e.* energy transfers below the quasifree peak.)

2.4 Motivation for Perpendicular Kinematics

Here, the focus would be on extraction of the R_{LT} response function. This response is expected to be sensitive to relativistic effects. Although covariant calculations have been performed for elastic ^{2}H(e,e') [25] and for ^{2}H$(e,e'p)n$ [6], they always involve some simplifying assumptions. It is necessary to test these assumptions.

Recent calculations of Jeschonnek, Donnelly and Van Orden [26, 27] suggest that

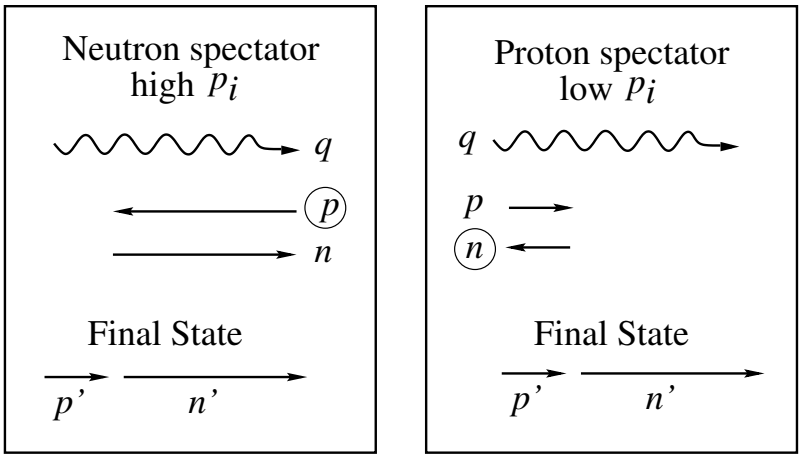

Figure 2: The proton and neutron are labeled p and n respectively. The struck particle in each case is circled. The final state momenta are indicated with primes. The left panel shows the situation when the proton is struck and the neutron is the spectator and vice versa for the right panel. Both situations lead to the same final state and are therefore experimentally indistinguishable. This illustrates that the proton spectator diagram, which corresponds to low initial momentum, can feed high p_r.

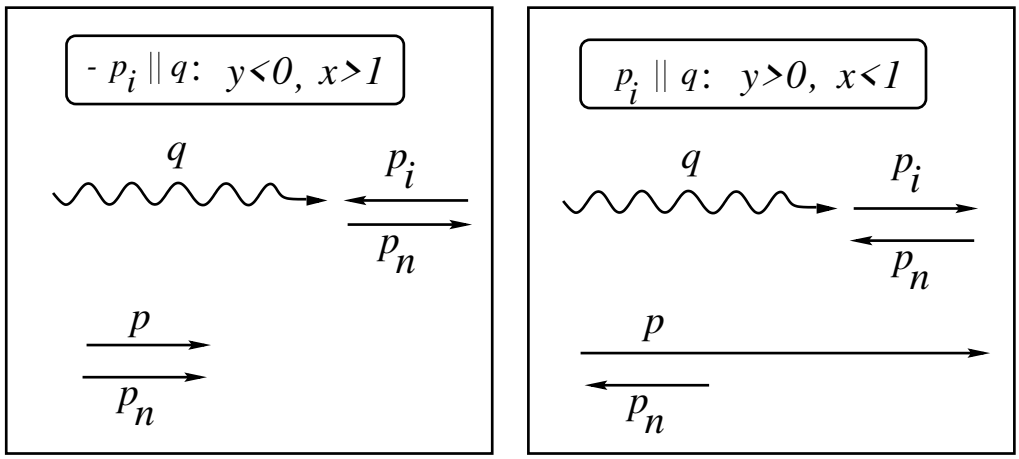

Figure 3: The left panel shows anti-parallel kinematics and the right shows parallel kinematics. In both cases it's assumed that the proton is struck so that $\vec{p}_i + \vec{q} = \vec{p}$. For illustrative purposes the left panel shows the situation for threshold breakup where the proton and neutron move off together with equal momenta. In this case, where $|\vec{q}| = 2|\vec{p}_i|$, the virtual photon effectively reverses the proton momentum leading to a small energy transfer (compared with the right panel).

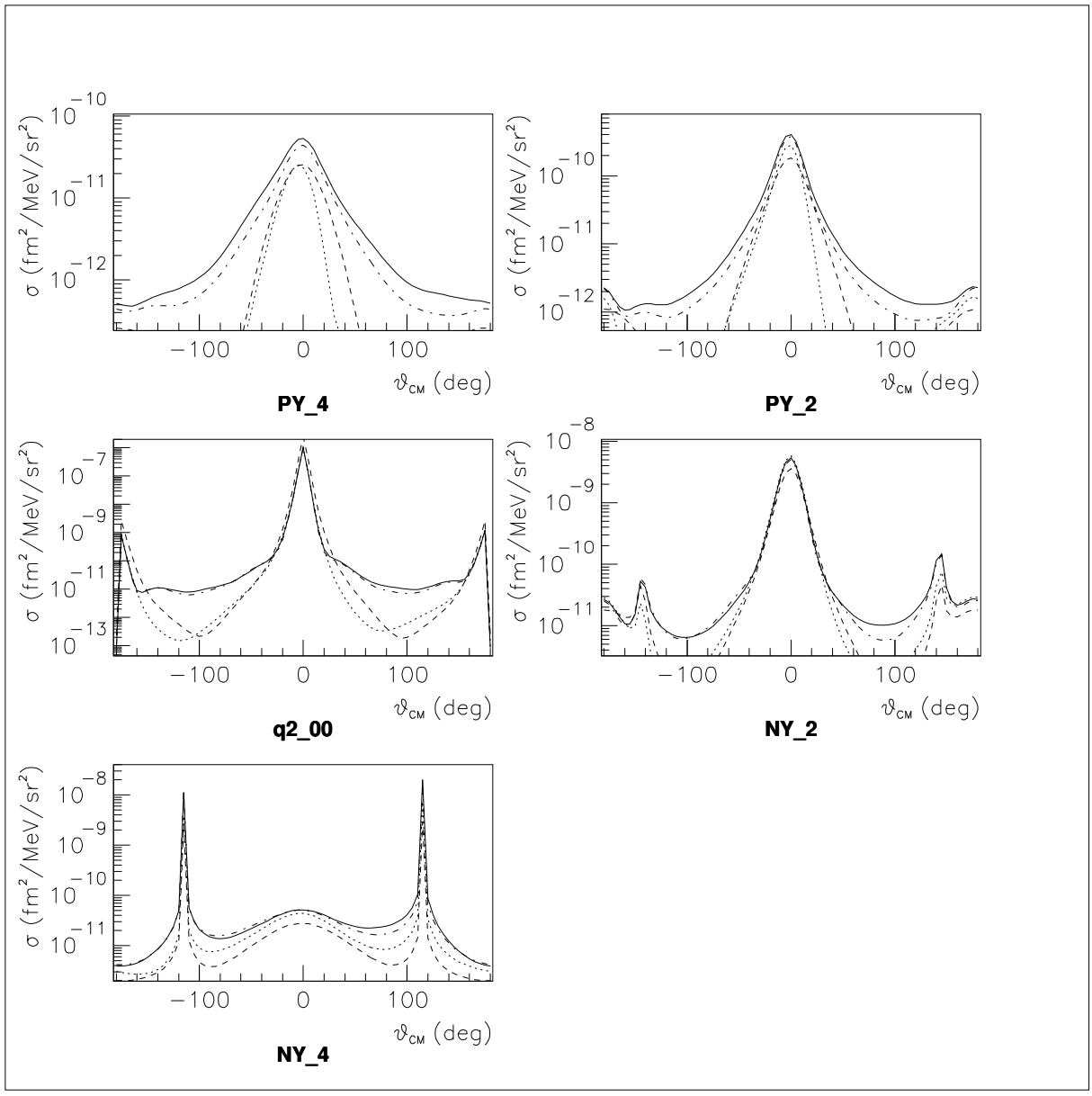

Figure 4: Calculations of the cross section for ^{2}H$(e,e'p)n$ by Arenhövel for a sample of the parallel/anti-parallel kinematics measurements (see the text for explanation of the labels of each panel). The dashed curve is PWBA, the dotted curve includes relativistic corrections, the dot-dashed curve includes also FSI and the solid curve is the full result which includes also MEC and IC. Reading from left to right and then down the page, the energy transfer monotonically decreases. The sharp structures on the wings of the spectra result from singularities in the proton CoM to Lab solid angle Jacobian.

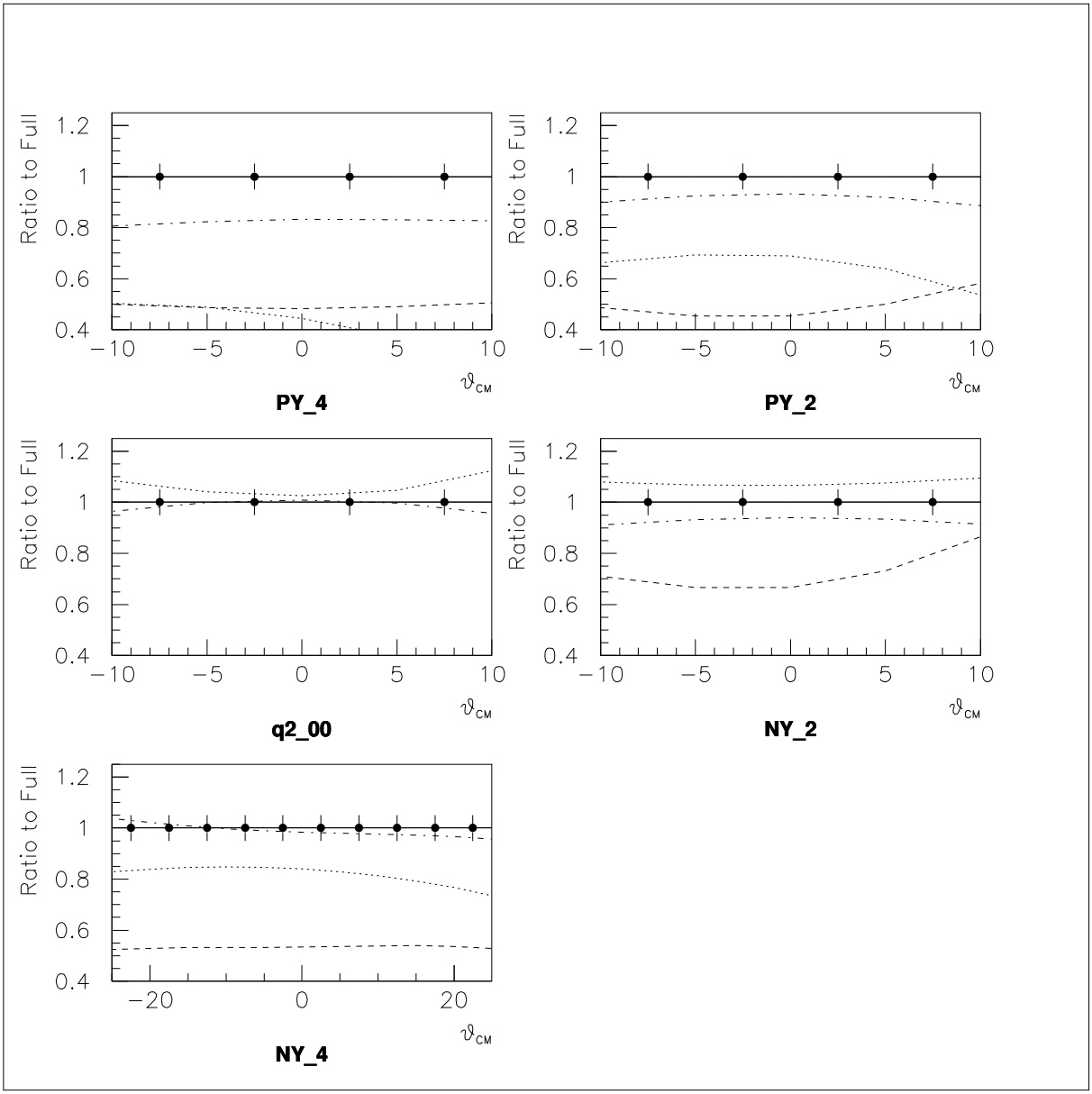

Figure 5: The ratio of each of Arenhövel's curves shown in Figure 4 to the full result. The labeling of the curves is the same as in Figure 4. The projected data are shown with 5% uncertainties per bin, which is an estimate of the systematic error. The statistical uncertainties per bin are smaller than this 5% and are, in most cases, negligible in comparison.

the bulk of the relativistic effects may be in the nucleon current operator, as opposed to the nuclear dynamics. They obtained good agreement between a manifestly covariant calculation involving the Gross equation [25] and a calculation using a nonrelativistic wave function and a relativistic nucleon current operator. In contrast, a calculation with a nonrelativistic wave function and current operator drastically failed to reproduce the results of the covariant calculation. This highlights the importance of doing a proper relativistic treatment. Further, if, indeed, the relativistic effects are mostly in the current operator, they can be incorporated for heavier nuclei using the same approach. Due to its more tractable nature, the deuteron provides a testing ground for such an approach.

The PWBA model of refs. [26, 27] has been applied to the kinematics of this proposal and results for the highest and lowest Q^2 kinematics are shown in Figures 6, 7, 8 and 9. In addition, for the middle Q^2 kinematics, the Jeschonnek *et al.* calculations are compared to calculations of Arenhövel [24] in Figures 10, 11 and 12. The main conclusions to draw from this large mass of curves are:

- The differences between the non-relativistic and relativistic calculations for R_{LT} are extremely large, even at the lowest Q^2. Both the Jeschonnek and the Arenhövel calculations show this.

- The differences between the relativistic Arenhövel and Jeschonnek calculations are significant. This is seen in Figure 11.

- The D-state becomes very important for the higher values of θ_{cm}. Thus, the R_{LT} can provide constraints on the D-state and hence the NN tensor force.

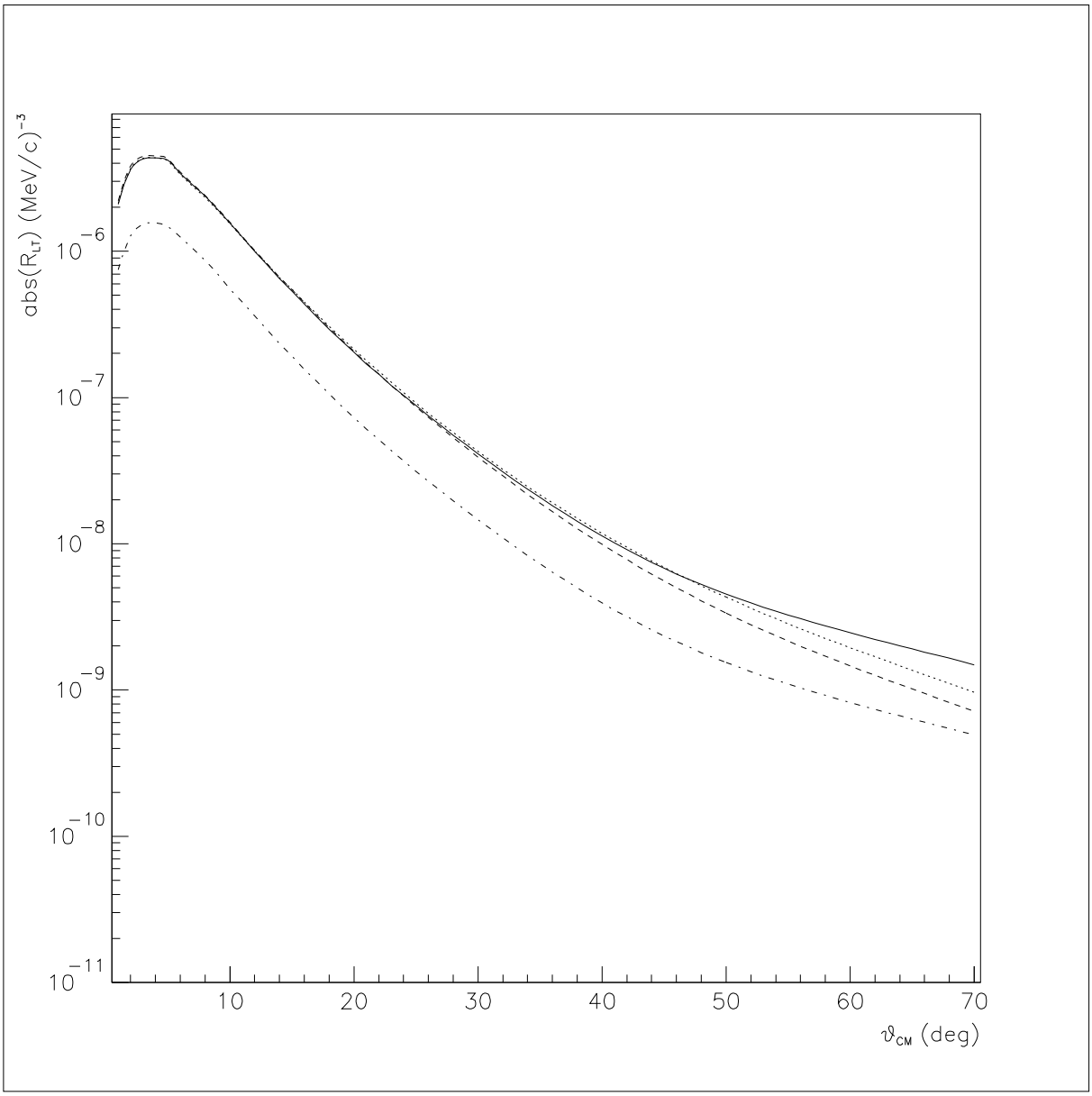

Figure 6: Calculations based on the PWBA code of Jeschonnek *et al.* for $|R_{LT}|$ for the lowest Q^2 measurement of this proposal. The solid line is for the Argonne V18 wavefunction, the dashed line is for the Bonn wavefunction, the dotted line is for the CD-Bonn wavefunction, and the dot-dashed line is for the non-relativistic calculation.

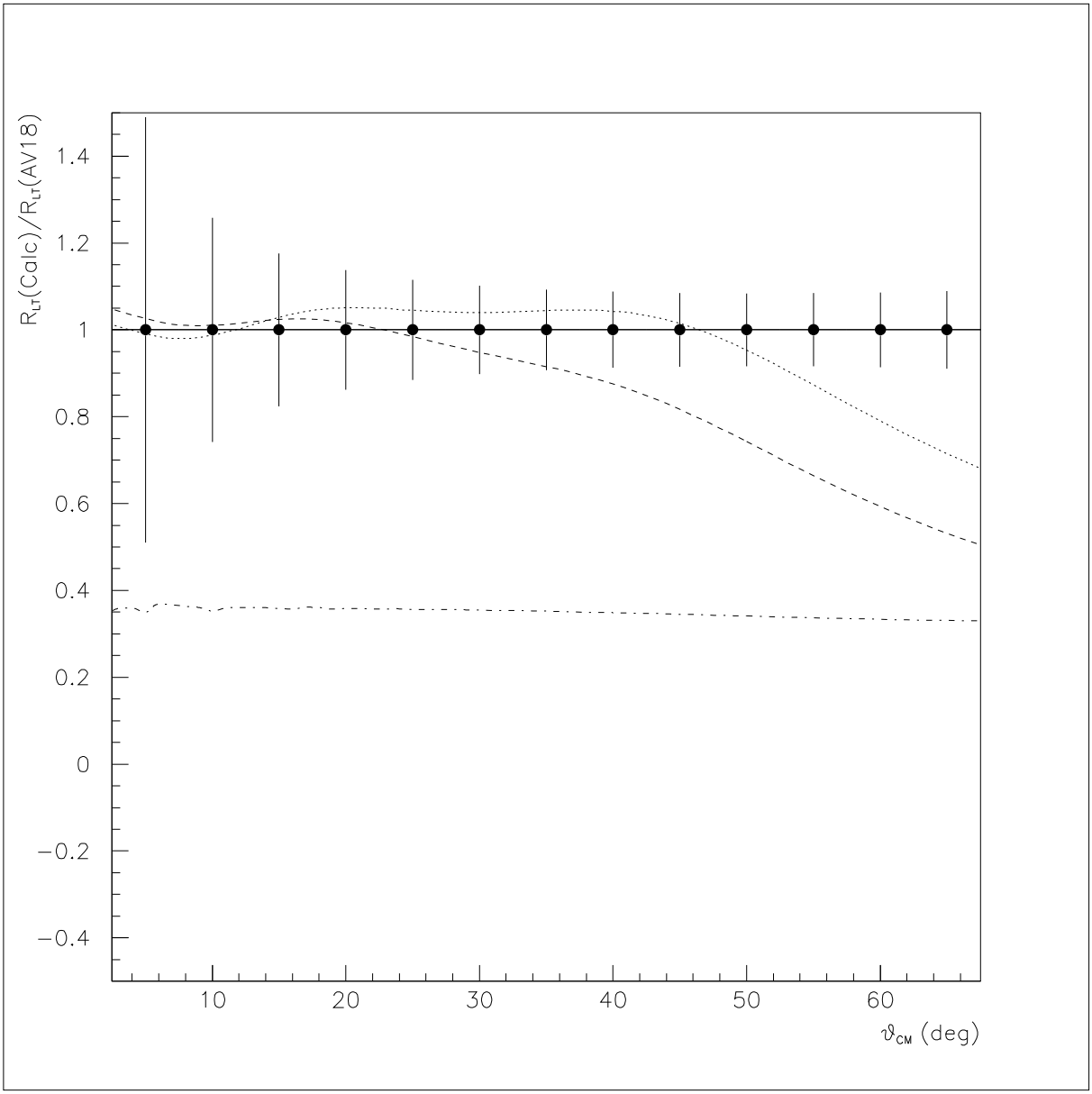

Figure 7: The ratio of each of the curves of Figure 6 (lowest Q^2 setting) to the Argonne V18 result. The curves labels are the same as for Figure 6. The projected data for this proposal are shown with 5% uncertainties in the cross sections which is an estimate of the overall systematic error. The statistical errors per bin are smaller than this 5% and, in most cases, negligible in comparison.

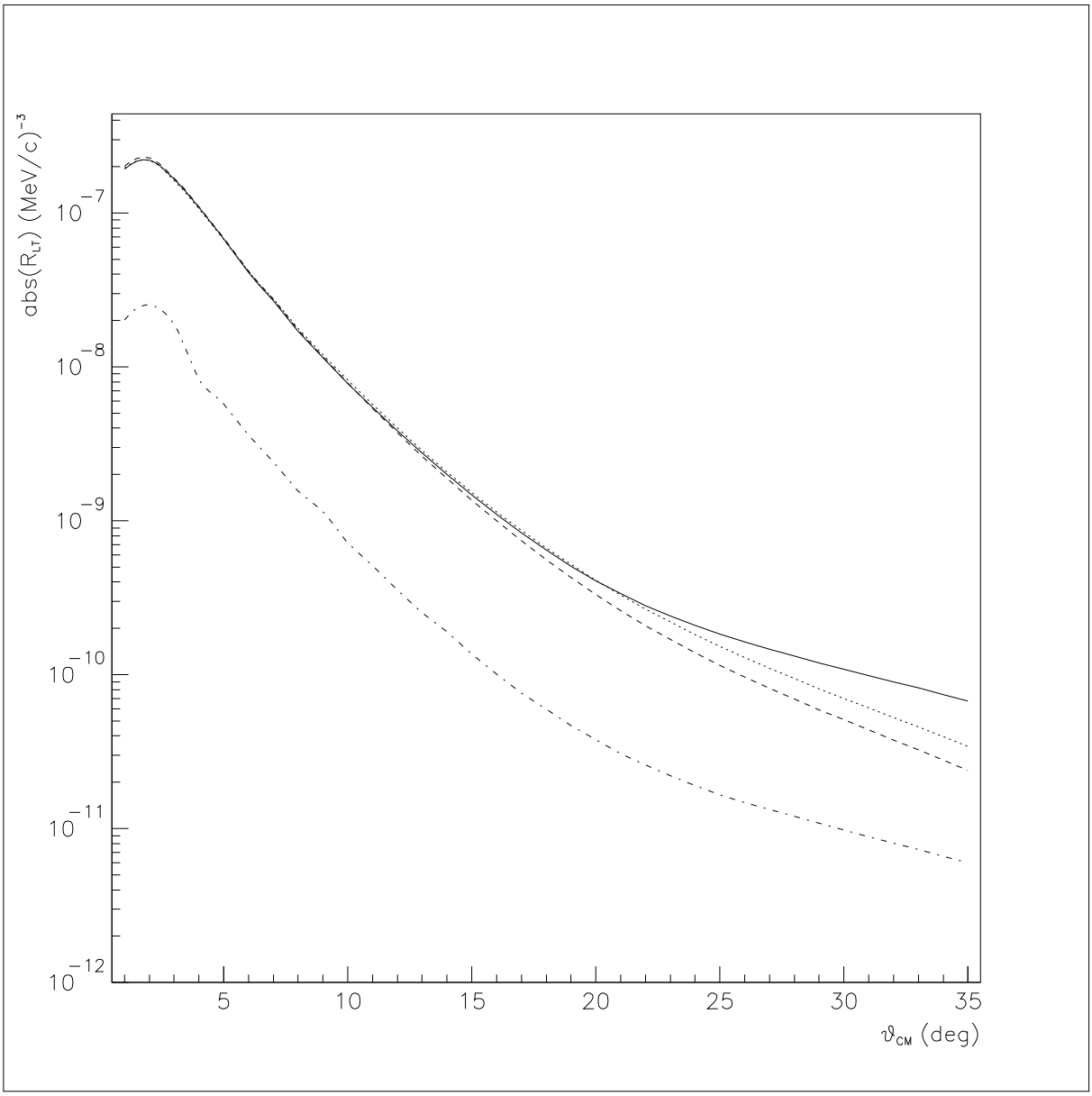

Figure 8: Same as Figure 6 except for the highest Q^2 kinematics.

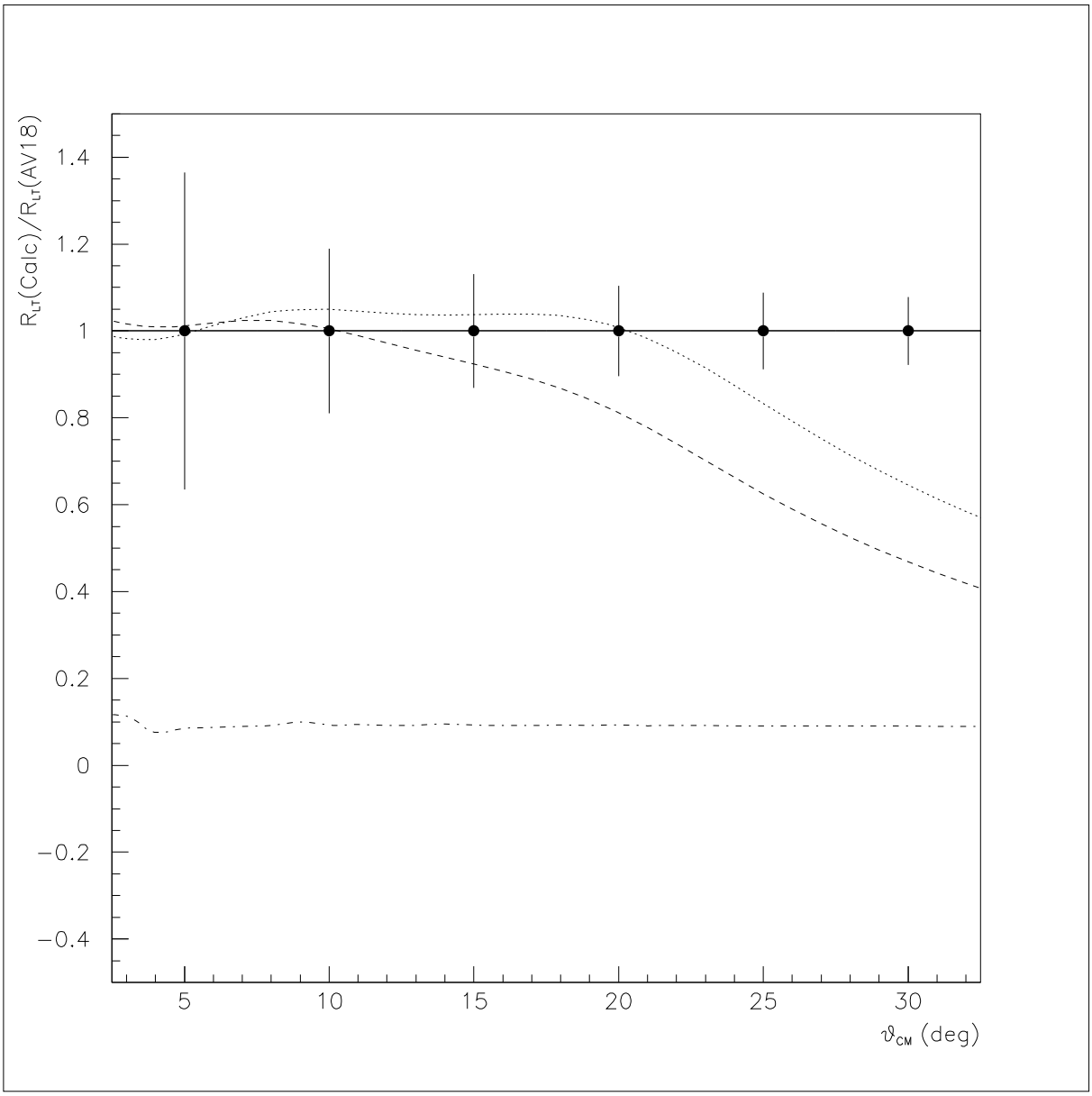

Figure 9: Same as Figure 7 except for the highest Q^2 kinematics.

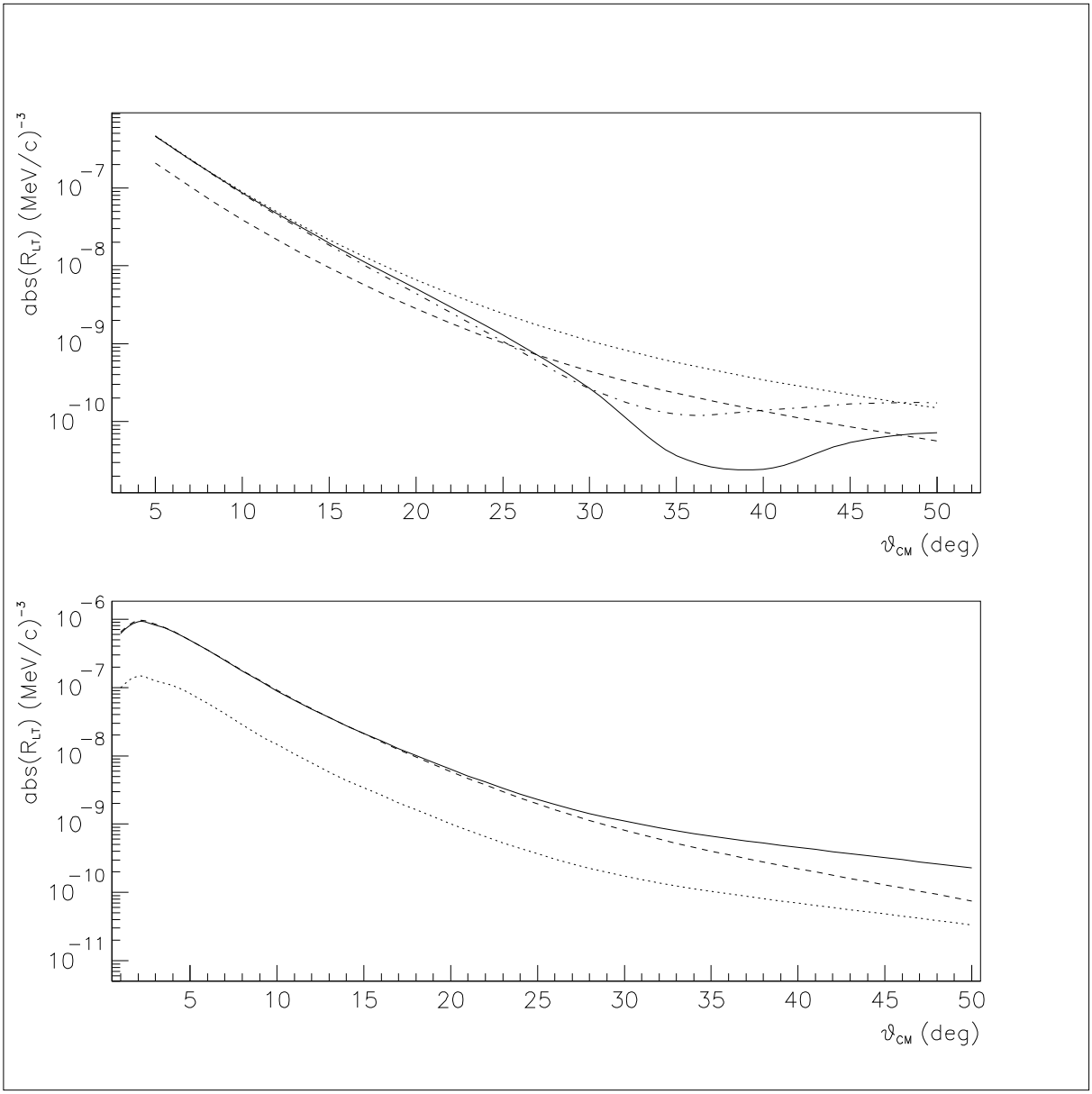

Figure 10: Upper panel: Calculations of Arenhövel for the middle Q^2 kinematics. The dashed curve is PWBA, the dotted curve includes relativistic corrections, the dot-dashed curve includes also FSI and the solid curve is the full result which includes also MEC and IC. Lower panel: Calculations based on the PWBA code of Jeschonnek *et al.* The solid curve uses the Argonne V18 wavefunction, the dashed curve uses the Bonn wavefunction, and the dotted curve is the non-relativistic result.

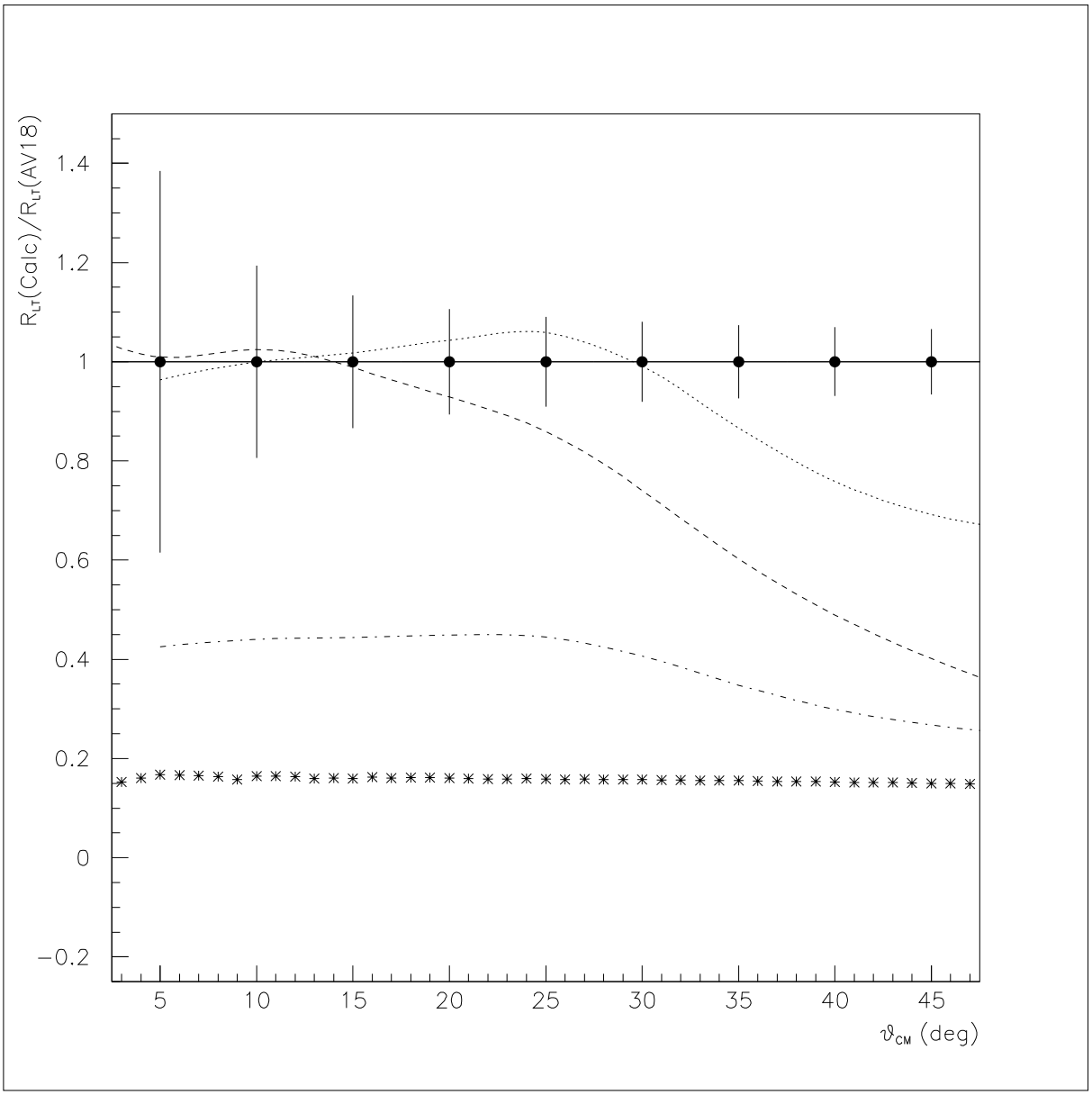

Figure 11: Calculation of Arenhövel and calculations based on the PWBA code of Jeschonnek *et al.* for the middle Q^2 kinematics. The solid curve is the Jeschonnek result using the Argonne V18 wavefunction, the dashed curve uses the Bonn wavefunction, the asterisks are the non-relativistic result, the dotted curve is the result of Arenhövel's PWBA calculation with relativistic corrections using the Bonn wavefunction and the dot-dashed curve is Arenhövel's non-relativistic result. The curves have each been normalized to the Argonne V18 curve. The projected data are shown with an overall 5% error per bin in the cross sections.

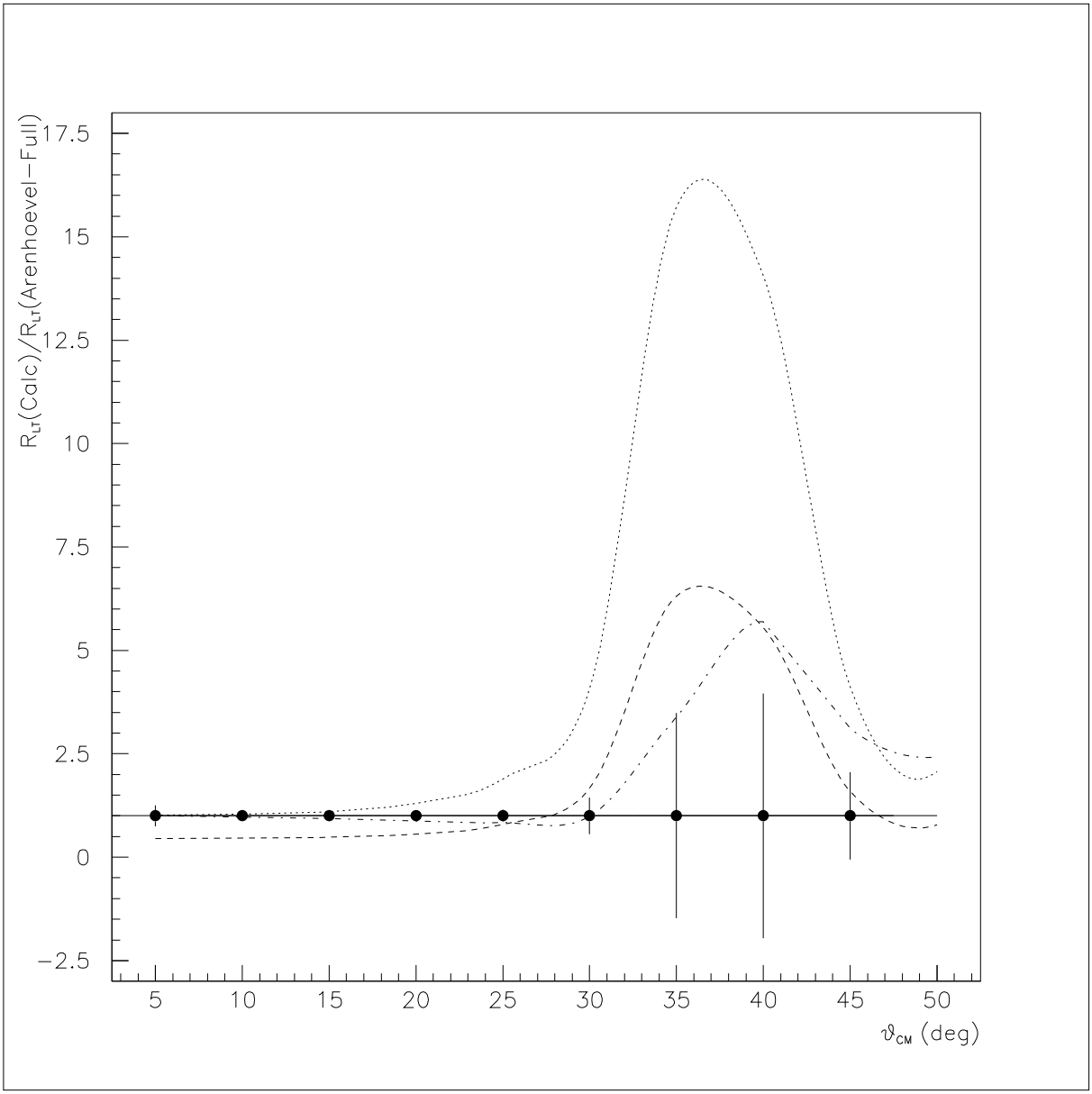

Figure 12: Calculations of Arenhövel for the middle Q^2 kinematics. The dashed curve is the PWBA calculation and the dotted curve includes relativistic corrections. The dot-dashed curve includes also FSI and the solid line is the full result including also MEC and IC. Each curve has been normalized to the full result. The projected data are shown with an overall 5% error per bin in the cross sections.

3 Physics Motivation: Angular Distribution

The understanding of the short-range structure of the bound two-nucleon system - the deuteron, is of fundamental importance for the advancement of the theory of nuclear matter at short distances. To probe the short-range properties of the deuteron one has to investigate configurations where the two nucleons come very close together and are essentially strongly overlapping. The basic problem is to what extent these configurations can be described in terms of two nucleons with high initial relative momenta (Fermi momenta). Traditionally three classes of reactions are used to study the high momentum part of the deuteron wave function: elastic scattering, inclusive and exclusive electro-disintegration reactions.

Elastic electron-deuteron scattering at large transfered 4-momentum Q^2, being sensitive to the high momentum component of the deuteron wave function, probes the integrated characteristics of the wave function via the deuteron form-factors. The analysis of the recent experimental data [28] showed that, at presently available energies, it is practically impossible to discriminate between different theoretical approaches [29] used to calculate the deuteron elastic form-factor $A(Q^2)$. The main problem is the lack of an independent determination of the deuteron wave function at large nucleon momenta (i.e. short distances).

Inclusive, inelastic (e, e') reactions provide a more direct way of probing high momentum components of the deuteron especially at high Q^2 and in the $x \geq 1$ regime [30]. In this regime the measured cross section is sensitive to the longitudinal component of the deuteron momentum distribution with respect to the virtual photon momentum $\vec{q}$. However the impossibility to isolate inelastic (nucleon) contributions (growing with Q^2) and final state interactions at large x (see e.g. [31, 32, 33]), preclude a direct access to the deuteron wave function at short inter-nucleon distances (although the high-momentum component is certainly important in this kinematics).

The most direct way of studying high nucleon momenta is to investigate the quasi-elastic electro-disintegration of the deuteron via the ^{2}H$(e, e'p)$ reaction at high missing momenta p_{miss} . Within the Plane Wave Impulse Approximation (PWIA) p_{miss} corresponds to the initial momentum of the target nucleon before the interaction. Thus the strategy in these studies is to probe the cross section at p_{miss} values as large as possible. However, depending on the selected kinematics, these studies can be overwhelmed by inelastic (meson and Δ-isobar) channels. This has been confirmed by early experiments at low/intermediate energies of scattered electrons [34]. Also more recent experiments [35] at slightly higher energies and momentum transfers found that in the regime of large p_{miss} medium/long range (soft) two-body currents such as meson-exchange currents and isobar contributions significantly dominate the cross section. In general, to suppress processes due to large inter-nucleon distances and to enhance contributions of reaction mechanisms which probe the short-distance structure of the deuteron, *the transfered momentum in the reaction should typically be larger than 1 GeV/c.*

This experiment proposes to measure the coincidence cross section for the electro-disintegration of the deuteron

$$e + d \rightarrow e' + p + n \tag{1}$$

at four momentum transfers of Q^2 = 0.8, 2.1 and 3.5 (GeV/c)^2 and missing momenta of p_{miss} = 0.2, 0.4 and 0.5 GeV/c. These measurements will be carried out in quasi-elastic kinematics for which we use the notations: q=$(q_0, \vec{q})$ for the 4-momentum of the virtual

photon ($Q^2 = q^2 - q_0^2$), and p_d=$(m_d, \vec{0})$ and p_f=$(E_f, \vec{p}_f)$ for the target deuteron and the detected nucleon 4-momenta respectively. For each value of Q^2 and p_{miss} the angle of the recoiling neutron, with respect to the momentum transfer, will be varied to build a complete angular distribution of the differential cross section over the full available phase space. As shown in the following sections, this will provide the necessary experimental information on the ^{2}H$(e, e'p)$ reaction at high Q^2, covering both $x < 1$ and $x > 1$ regions, to allow us to address the problems of:

- the Final State Interactions (FSI) between knock-out and recoil nucleon,
- the Meson-exchange Currents (MEC) and Isobar Current (IC) contributions,
- and the dynamics of the bound two nucleon system.

The quantitative understanding of these processes is the inescapable preliminary step towards the study of the Short Range NN Correlations (SRC) in the deuteron and the eventual manifestation of non-nucleonic/quark-gluon degrees of freedom in this nucleus.

A comprehensive program of experimental studies of high Q^2 electro-disintegration of the deuteron will have a significant impact on our understanding of the structure of the NN interaction at short-distances. Measurements of the ^{2}H$(e, e'p)$ cross section in a wide range of missing momenta, recoil nucleon angles, and the virtuality of the exchanged photon will allow us to eventually disentangle the different processes contributing to this reaction that are currently discussed in the literature.

3.1 Final State Interactions

Within PWIA, the out-going nucleon does not interact with the residual system after the interaction with the virtual photon. However in the kinematic region where one expects to have an enhanced contribution from SRC one may also expect a substantial contribution from FSI between the knock-out and the spectator nucleon. The main effect introduced by FSI is that the nucleon momentum (say $\tilde{p}_{miss}$), carried by the bound nucleon before the interaction with the electron, is not the same as the one measured in the experiment $\vec{p}_{miss} = \vec{p}_f - \vec{q}$. As a result one can not be confident that the condition of large p_{miss} , automatically guarantees that high momentum components in the ground state wave function of the deuteron are measured. In all previous ^{2}H$(e, e'p)$ experiments at large p_{miss} the FSI were a major contributor to the overall cross section and therefore substantially overshadowed SRC.

With increasing energies, the situation changes qualitatively. At large angular momenta, FSI are dominated by the pn re-scattering and then become strongly anisotropic with respect to the direction of $\vec{q}$. The maximal re-scattering happens in directions almost transverse to $\vec{q}$. Consequently, FSI contribute much less for parallel and anti-parallel kinematics and can be treated there as a correction. *However this phenomenon has still to be observed experimentally for the $^2H(e, e'p)$ reaction.*

The dominance of large angular momenta allows to apply eikonal approximations in calculating FSI. A well known example of the eikonal approximation of FSI is the Glauber approximation [36]. However the latter was derived for cases where one can neglect the motion of bound nucleons in the nucleus. For the ^{2}H$(e, e'p)$ reaction at large missing momenta, the eikonal approximation was generalized (GEA) in order to account for finite values of nucleon momenta [37, 38]. Fig. 13 represents the ratios of the calculated cross

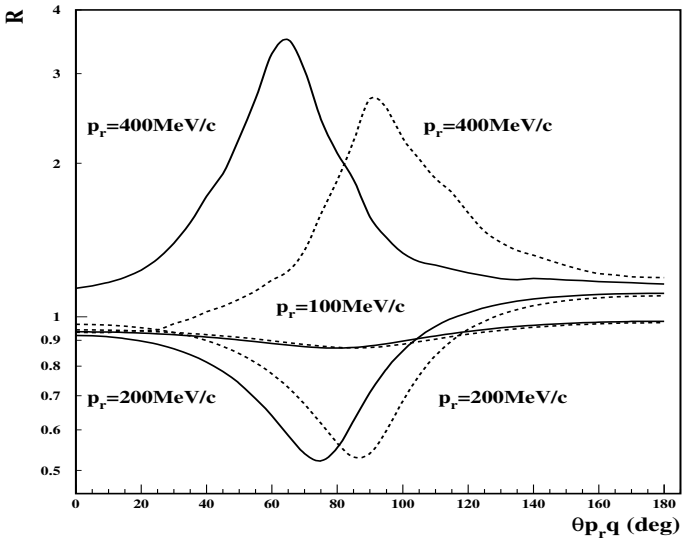

Figure 13: The angular dependence of R, the ratio of the D(e,e′p)n cross section calculated including PWIA and FSI terms to the cross section which includes PWIA term only: GEA (solid line) and according to the conventional Glauber approximation (dashed line).

sections that include FSI to the one within PWIA only. The ratios are shown for different values of recoil momenta as a function of the angle between the recoiling nucleon and $\vec{q}$. The calculations here are carried out within the conventional Glauber approximation and the generalized Glauber approximation (GEA). It is shown that while being similar at small values of p_{miss} the predictions substantially diverge at larger p_{miss} values.

The eikonal approximation is expected to become decreasingly valid for smaller energies. Indeed, when the center of mass energy of the final pn system decreases, the relative momenta in the pn system become small and the eikonal approximation should break down to let place to an intermediate energy regime. However, it is not clear at which Q^2-value the transition between these two regimes takes place. Data from an experiment on nucleon propagation in the A(e,e'p)X reaction [39, 40] indicates that this transition happens already at 1 (GeV/c)^2. However these data are taken for small values of p_{miss} $\leq$ 200 MeV/c and it is quite likely that this transition depends on p_{miss} , especially for the $x \geq 1$ kinematics ($\theta_{\rm prq} < 90^\circ$ in Fig. 13). A comparison [37] of calculations carried out within the medium energy approach [41], in which the pn final state was calculated by summing all states with angular momenta $l \leq 7$, and the GEA, indicates that for the case of larger p_{miss} the transition happens already at $Q^2 \approx 1$ (GeV/c)^2. This is confirmed by the diagrammatic approach of Laget [42], which deals with interaction effects (FSI, MEC, IC) without kinematical approximations. The kinematics is relativistic, and the full angular dependency of the elementary operator is kept in the loop integrals. Only positive energy components of the wave functions are retained, and are parametrized by solution of the Lippman-Schwinger equation for the Paris Potential (the argument of the bound state wave function is the relativistic momentum of the spectator nucleon). The elementary electromagnetic operator is expanded in power of p/m, up to and including term in $(p/m)^4$ [43]. Instead of the partial expansion of the nucleon-nucleon scattering amplitude [42, 43], the model is extended to high energy by parameterizing the scattering

amplitude as $\propto \sigma_{NN} \exp(bt)$, with the experimental values of σ_{NN} and b [44, 45]. Fig. 14 shows that the peak in the FSI occurs at the same place as in the GEA treatment. It is a straight forward consequence of unitarity, as its maximum occurs when on-shell scattering is maximized in the FSI loop integral at $x = Q^2/2m\nu = 1$.

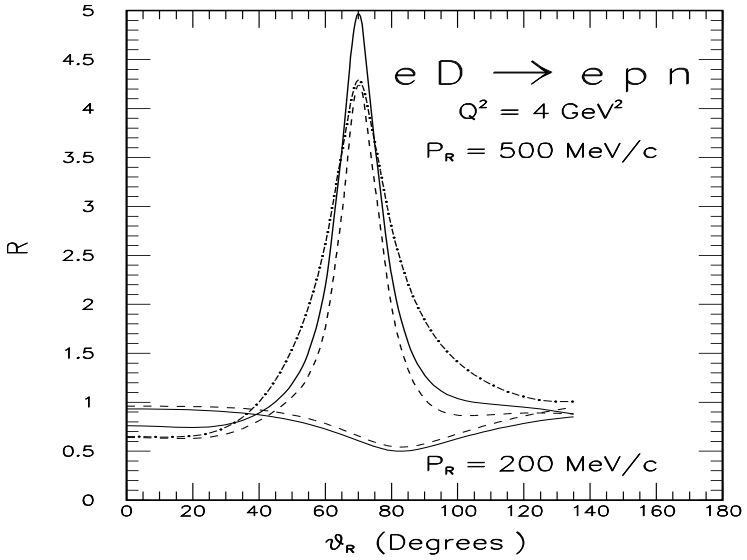

Figure 14: The angular dependence of the ratio of the D(e,e'p)n cross section calculated within different approaches to the cross section including PWIA term only: factorized PWIA+FSI (solid lines) and unfactorized PWIA+FSI (dashed lines).

Finally, a measurement of the ^{2}H$(e, e'p)$ cross section as a function of the angle of the recoiling nucleon will indicate those regions where FSI can be factorized from the initial $\gamma^* N$ interaction. These regions are very important for isolating the physics related to the $\gamma^* N$ interaction (EMC type phenomena) from the one related to the physics of the NN interaction at large $Q^2 \geq 4$ (GeV/c)^2 (Color Transparency). An advantage of the deuteron is that unfactorized calculations can be realized in a straightforward way depending upon certain assumptions on the structure of NN interaction. One such calculation based on the conventional Glauber approximation [46] has been carried out in Ref. [47]. A quantitative estimate of the effects of factorization has been performed in the framework of Laget's approach. As demonstrated in Fig. 14, they are not important and do not alter significantly the shape and the magnitude of the rescattering peak. On the other hand, the scattered proton can be off-shell. Contrary to the on-shell part, this part of the rescattering amplitude is model dependent, since it depends on the half-off-shell pn scattering amplitude which is poorly known in the GeV energy range. However, as can be seen in Fig. 14 the off-shell rescattering contribution does not affect the height of the FSI peak (it vanishes here), while it slightly broadens its tails. Fig. 15 compares the three different approaches. When off-shell pn rescattering is allowed, the Laget approach is very similar to the GEA. In the following only the iron clad on-shell rescattering has been retained in Laget's approach. The measurements of the ^{2}H$(e, e'p)$ cross section at $p_{miss} \geq 0.4$ GeV/c will be able to provide important new information about these issues.

This experiment proposes to address these problems by measuring, for several Q^2 and

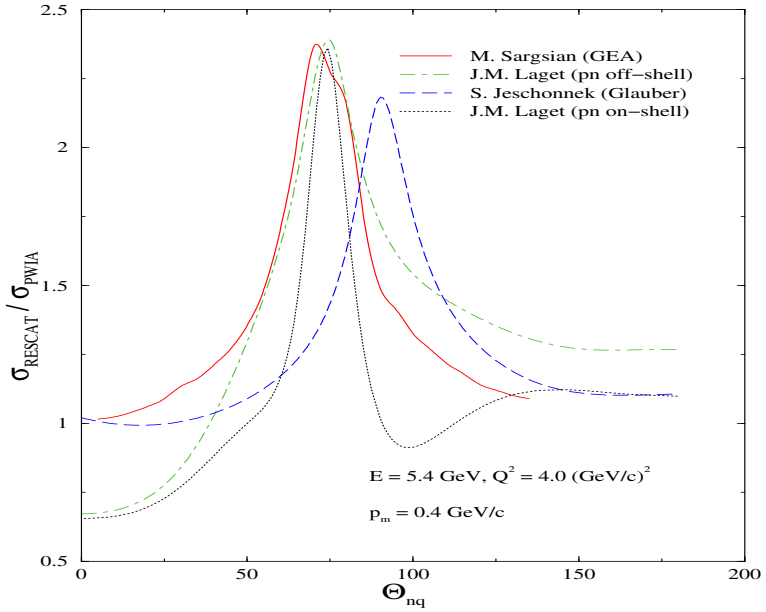

Figure 15: The ratio between the ^{2}H$(e,e'p)$ cross section calculated including FSI and PWIA for Q^2 = 4 (GeV/c)^2 and p_{miss} = 0.4 GeV/c.

recoil angles, a ratio like

$$R(Q^2,\theta_{\rm prq}) = \frac{\sigma(p_m = 0.2, 0.4, 0.5)}{\sigma(p_m^{ref.} = 0.05)} \tag{2}$$

which is the ratio of the cross section at given p_{miss} to the cross section at a small reference missing momentum for which the PWIA is valid. The study of the $\theta_{\rm prq}$ dependence of such a ratio at fixed Q^2 will allow to isolate FSI effects and investigate the factorization of the FSI and the $\gamma^* N$ interaction. An important goal of these measurements will be to confirm the theoretical expectation that FSI are generally suppressed in parallel and anti-parallel kinematics compared to perpendicular kinematics. The experimental verification of this prediction is very important since it might open a window to directly probe contributions of SRC to the nucleons wave function.

3.2 Meson Exchange Currents and Isobar Contributions

Experimental ^{2}H$(e,e'p)$ data at low Q^2 demonstrated that with increasing p_{miss} MEC and IC become dominant, making it virtually impossible to extract information on short-range NN correlations. The calculation of MEC and IC at high Q^2 is very complicated since the virtuality of the exchanged mesons greatly exceeds their masses. However it is possible to estimate the Q^2 -dependence of these contributions based on the analysis of the corresponding Feynman diagrams. Theoretically one expects that the MEC contribution will decrease with increasing Q^2. Indeed it can be shown that MEC diagrams have an additional $\sim 1/Q^2$ dependence compared to the diagrams where the electron scatters from a nucleon. This suppression comes from two major factors. Firstly, because at the considered kinematics the knocked-out nucleon is fast and takes almost the entire

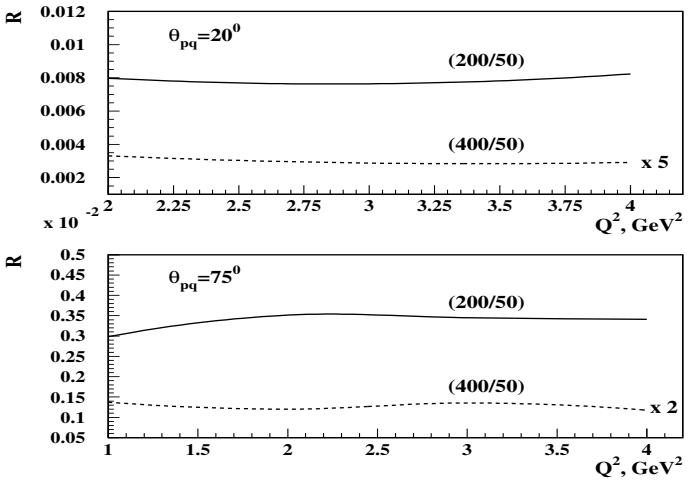

Figure 16: Q^2 dependence of the ratio R (Eq. 2) for p_{miss} =0.2−0.4 GeV/c and $\theta_{\rm prq} = 20-70^\circ$.

momentum of the virtual photon q, the exchanged meson propagator is proportional to $(1 + Q^2/m^2_{meson})$. Secondly, an additional Q^2 dependence comes from the $NN - meson$ form-factor $\sim (1+Q^2/\Lambda^2)$. Thus the overall additional dependence as compared to PWIA diagram is [48]

$$\frac{1}{(Q^2 + m^2_{meson})}\,\Gamma_{MNN}(Q^2) \propto \left(\frac{1}{(Q^2 + m^2_{meson})}\,\frac{1}{(1 + Q^2/\Lambda^2)^2}\right) \qquad (3)$$

where $m_{meson} \approx 0.71$ and $\Lambda^2 \sim 0.8 - 1$ (GeV/c)^2 [1]. Thus one expects that MEC contributions will be strongly suppressed as soon as $Q^2 \geq m^2_{meson}$ and $\Lambda \sim 1$ (GeV/c)^2. As can be seen in Fig. 16 the Q^2 dependence of the ratio R (Eq. 2) including FSI is very weak. This is confirmed by another estimate performed in Laget's approach (Fig. 17). At low Q^2, MEC and IC contribution is not negligible, as the invariant mass of the np system spans the baryonic resonance regime. Their contribution is clearly suppressed at higher Q^2. Note also that the MEC seem to be enhanced in the region of $\theta_{\rm prq} > 90^\circ$ which is covered by the proposed experiment. This is the region which is closely connected to the kinematics of the large angle $\gamma + D \to pn$ experiment where the MEC picture seems to break down at Q^2 values $\sim$1 (GeV/c)^2. In addition, the MEC contribution in the region of maximum FSI is shown to be small, making the projected measurement of FSI increasingly reliable.

Hence getting complementary data sensitive to MEC effects for large momentum transfers is very interesting. One may expect that in the long run such measurements would permit to discriminate between meson exchange [50] and quark exchange pictures [51] of large angle emission of nucleon pairs. To estimate the IC contribution, we observe that the $x < 1$ and $x > 1$ regions at the same p_{miss} have different contributions from intermediate Δ excitations. In this case the amplitude of the IC contribution

[1] We assume here that different meson-nucleon vertecies have a similar dependence on Q^2 . Assuming the dipole dependence on Q^2 corresponds to neglecting the size of a meson as compared to the size of a baryon (for large Q^2 quark counting rules lead to $\Gamma_{MNN}(Q^2) \sim \frac{1}{Q^6}$). We also use restrictions on the Q^2 -dependence of the πNN vertex from measurements of the antiquark distribution in nucleons [49].

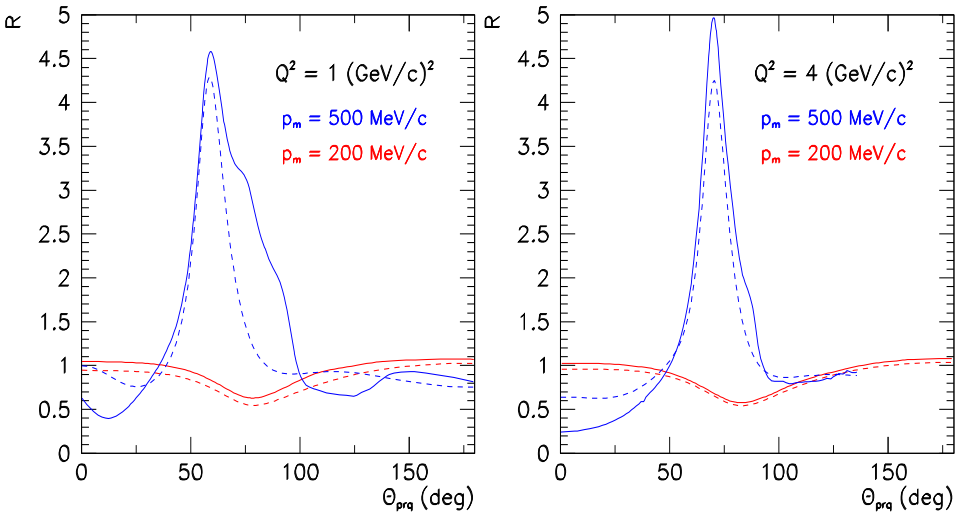

Figure 17: The angular dependence of R, the ratio of the D(e,e′p)n cross section calculated within different approaches to the cross section including PWIA term only: PWIA+FSI only (dashed curves), PWIA+FSI+MEC+IC (full curves).

is proportional to:

$$\psi_D\left(p_{mt}, p_{mz} - \frac{M_\Delta^2 - M_N^2}{2q}\right), \tag{4}$$

where p_{mt} and p_{mz} are the transverse and longitudinal components of the measured missing momentum. This equation shows that one can expect more IC contributions in the $x < 1$ region than in the $x > 1$ since in that case $p_{mz} - \frac{M_\Delta^2 - M_N^2}{2q} < p_{mz}$. Thus a combined study of the cross section at constant p_{miss} but different x regions will be sensitive to IC contributions in the overall cross section.

3.3 The Dynamics of Deeply Bound Nucleons

Once the contributions due to SRC are isolated, by deconvoluting from FSI+MEC+IC contributions, the fundamental question that remains is the dynamics of the electromagnetic interaction of deeply bound nucleons in SRC. The investigation of the cross section in near parallel $x < 1$ and anti-parallel $x > 1$ kinematics, where FSI are expected to be a correction, as discussed above, will yield important information about the structure of vacuum fluctuations. The problem here is that, with increasing missing momentum in nuclei the relative contribution of vacuum diagrams also increases. By vacuum diagrams one means the process where the virtual photon splits into a N$\bar{\text{N}}$ pair (Fig. 18). The $\bar{\text{N}}$ is subsequently absorbed by the nucleus, yielding the same final hadronic state, that the direct knock-out process would have produced. To solve this known theoretical problem, a number of theoretical prescriptions have been developed [52, 53]. One of the methods is the development of the Light Cone (LC) dynamics of nuclei, where the contribution of vacuum diagrams are effectively calculated in the LC reference frame [52]. As a result in this case (similar to the high energy scattering in QCD) the LC nuclear wave function of the nucleus which emerges [52, 54, 55], depends on the variables $p_{m+}/p_D^+ \equiv \alpha$ and

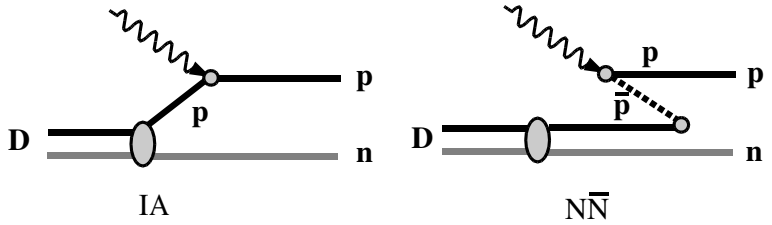

Figure 18: Impulse approximation (IA) and vacuum diagrams ($N\bar{N}$) diagrams for the electro-disintegration of the deuteron

p_{mt}. In the approximation when the deuteron is described as a two nucleon system there is an unambiguous connection between the LC and the non-relativistic wave function. In this case the LC wave function essentially depends only on the invariant mass of the two-nucleon system [52]. If mesonic degrees of freedom are included in the deuteron wave function, it depends on the two independent variables α, and p_{mt}, and can be explicitly calculated within particular models (see e.g. [56]). The overall cross section of the ^{2}H$(e,e'p)$ reaction is then the convolution of the off-p_{m-}-shell $\gamma^* N$ cross section and the LC deuteron wave function. Another description of the deeply bound nucleon is the virtual nucleon approximation [57], where the virtuality of the nucleon has been introduced while in the laboratory frame. In this case the PWIA cross section is expressed through a non-relativistic deuteron wave function and an off-energy(E_m)-shell γ^*N cross section. In the Laget's approach, an expansion in power of p/m is used, and no LC correction is made on the argument of the nuclear wave function. Up to $Q^2 \simeq 2.5$ (GeV/c)^2, this prescription is similar to the popular de Forest's one but it differs above. Today, there are many different approaches on how to treat the interaction of an electron with a bound nucleon at large Q^2 . *A dedicated measurement is mandatory to provide us with a guide in this matter.* Fig. 19 compares the cross sections calculated with the LC and virtual nucleon

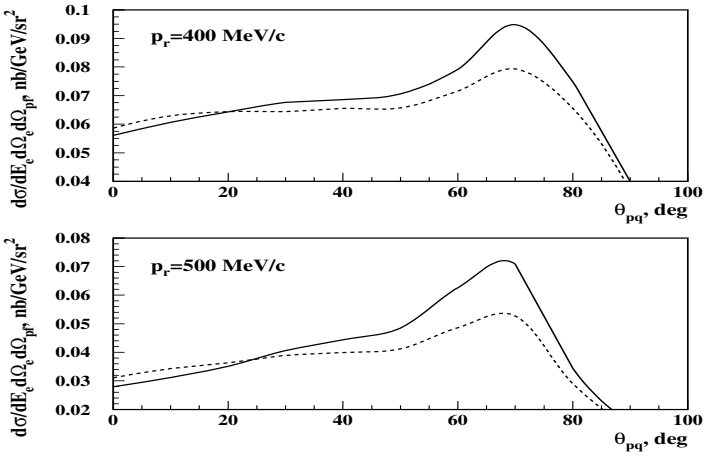

Figure 19: Angular dependence of the ^{2}H$(e,e'p)$ cross section calculated with the virtual nucleon (solid line) and the light cone (dashed line) approximations for Q^2 =4.0 (GeV/c)^2

approximations. It shows that for small recoil angles the two approaches predict very similar cross sections. This should therefore allow us to directly measure the deuteron

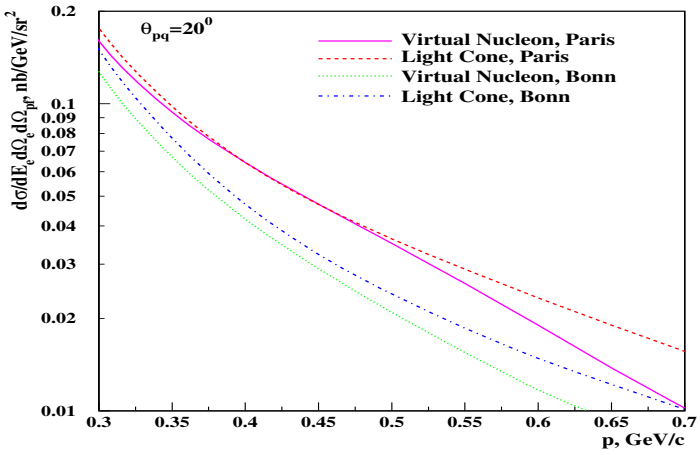

Figure 20: The ^{2}H$(e,e'p)$ cross section for $\theta_{\rm prq} = 20^\circ$ calculated within the virtual nucleon and the light cone approach.

wave function. As an example Fig. 20 shows cross sections calculated using wave functions based on the Paris and the Bonn potentials. It is very important that these comparisons will be done at fixed values of Q^2 which will enable us to isolate the effects related to the modification of the deeply bound nucleon's quark-gluon wave function (similar as in EMC-type effects). The p_{miss} dependence of the ratio of the ^{2}H$(e,e'p)$ cross section in parallel ($x > 1$) and anti-parallel ($x < 1$) kinematics measured at lower and higher values of Q^2 will test the form-factor modification of deeply bound nucleons.

3.4 A Look Into the Future

Upon the quantitative understanding of the role of FSI, MEC, and IC in the electro-disintegration of the deuteron, one can start to address the important question of quark-gluon degrees of freedom in the deuteron.

The following projects may be part of a future experimental program, however, the proposed experiment might allow us first glimpses of these physics issues.

3.5 Onset of Quark-Gluon Degrees of Freedom

Upon verification of the smallness of FSI in (near) parallel and anti-parallel kinematics, the measurements of the cross section at larger values of p_{miss} (up to 700 MeV/c), where one expects that the two nucleon picture of the nucleon may still be valid, allows to study the nature of the core of the NN interaction. It is well known that the wave function of the deuteron diverges substantially in the region where the large repulsion of the NN interaction becomes important when calculated using different parameterizations of the NN potential. One of the reasons for this is that the current models do not fit phase-shifts in the region $T_N \geq 300$ MeV were meson production is allowed and which is very important for the calculation of the deuteron wave function for $k \geq 0.5$ GeV/c.

The high Q^2 domain and the $x > 1$ region allow to explore the very large missing momenta region where we expect that the nucleonic picture of the deuteron will break down. The onset of quark degrees of freedom will be dominated by quark-interchange

mechanisms in short range interactions. Although it is impossible at this point to predict the absolute values of such contributions, the scenario for a different number of quark exchanges will provide different deuteron momentum distributions.

Extending the cross section measurement to the region of high and very high missing momentum ($p_{miss} > 700$ MeV/c) will allow to reach the region where quark-exchange diagrams play a dominant role in SRC in the deuteron.

3.6 Quark-Gluon Structure of Deeply Bound Nucleons

Experiments of inclusive Deep Inelastic (DIS) electron scattering from nuclei demonstrated the modification of the nucleon quark-parton density as compared to that of the free nucleon (the EMC effect [58]). This effect unambiguously demonstrated that nuclei can not be described merely as a collection of unmodified nucleons. Moreover the proportionality of the EMC effect to the nuclear density was an indication that the modification of the quark-parton structure of nucleons depends on how strong nucleons are bound in a nucleus. Although the effect is observed in the DIS region, one should expect a similar modification for the elastic form-factors of bound nucleons. However, inclusive data alone will not allow one to conclusively check the existence of EMC type phenomena for the elastic form factors. One problem is that with the increase of Q^2, inelastic channels dominate the inclusive cross section and are thus obscuring elastic contributions [33].

One mechanism of the bound nucleon's form-factor modification is described in the color screening model [59, 60], where at sufficiently high values of $Q^2 \geq Q_0^2$ ($Q_0^2 \approx$2-3 (GeV/c)^2) the nucleon form-factor becomes sensitive to quark correlations. In this regime the bound nucleon will have suppressed quark correlations as compared to the free nucleon. The reason of such a suppression is the color-screening between quark-correlations which tends to minimize the nuclear binding. In this model the bound nucleon form-factor in the regime of scattering off a small size configuration is suppressed by a factor f:

$$f = 1 \Big/ \left[1 + \frac{(k^2 + m_N \epsilon_D)}{m_N \Delta E}\right]^2 \tag{5}$$

where $\Delta E \sim m_{N^*} - m_N \sim 600$ MeV and k is the spectator momentum. This factor strongly depends on k and hence could be tested in the discussed process. Note here that some indications of such an effect were found [61] in the $x > 1$, $Q^2 \geq 4$ (GeV/c)^2 kinematics for the SLAC $x > 1$ data. In parallel and anti-parallel kinematics where FSI are small, one can search for the possible bound nucleon modifications, by measuring the p_{miss} dependence of the ratio of two ^{2}H$(e, e'p)$ cross sections measured at the same $\vec{p}_m$ but different values of Q^2 ($Q_2^2 \geq Q_0^2$ and $Q_1^2 \leq Q_0^2$).

4 Experimental Program

We will measure the ^{2}H$(e,e'p)$ cross section and separate the R_{LT} response function at Q^2 = 0.8, 2.1 and 3.5 (GeV/c)^2. At each momentum transfer the ^{2}H$(e,e'p)$ cross section will be measured for a range of recoil momentum. Further, at p_{miss} = 0.2, 0.4 and 0.5 GeV/c the neutron angular distribution will be measured.

The kinematics for the low, middle and high Q^2 measurements are given in Tables 2, 3 and 4 respectively. The coincidence rates for proton spectrometer settings forward of $\vec{q}$ are typically significantly smaller than for settings backward of $\vec{q}$. This mainly stems from the asymmetrical way in which the $\vec{q}$ vector is populated (the Mott cross section decreases with increasing scattering angle which implies that the event population favors $\vec{q}$ backward of its central value). Therefore, for the two lower Q^2 settings, an asymmetric range of proton settings about $\vec{q}$ results. Only the overlapping range of p_{miss} will be used to extract R_{LT}.

Keeping the recoil momentum constant, the angle of the recoiling neutron with respect to $\vec{q}$ will be varied. For p_{miss} =0.2 GeV/c and p_{miss} =0.4 GeV/c the recoil angle will be varied between in the domains 20° - 150° and 20° - 110° respectively. This corresponds to a variation in x-Bjorken between typically 0.7 and 1.5. This variation of the neutron angle allows us to study in detail the effect of final state interactions as has been outlined in the previous sections. Small recoil momenta of the order of 50 MeV/c will be measured as a normalization measurement since at these values, contributions of FSI, MEC and IC are small. This has been confirmed by measurements at much lower Q^2 values [35, 39, 16].

As can be seen in Fig. 21 at p_{miss} =0.2 GeV/c, FSI reduce the cross section by approximately a factor of two at a neutron angle around 70° while at p_{miss} =0.4 GeV/c the cross section is enhanced by a factor of about 2.5 and an even larger factor at higher missing momenta. It is the goal of this experiment to measure this behavior qualitatively and quantitatively for various Q^2 values. We will measure the cross section in a bin of missing momentum of ± 20 MeV/c and in a bin of $\theta_{nq} = \pm 5°$ for the recoil angle (the angle between the recoiling neutron and the momentum transfer) with an expected statistical precision of 5 %. In the region of the large cross section enhancement, data will be taken in θ_{nq} steps of 10° . This should permit us to extract the location and the strength of this structure for various momentum transfers.

Fig. 22, 23 and 24 show the calculated cross sections with and without FSI effects. The points with error bars indicate the projected experimental data including statistical errors. Since no previous experiment has been carried out in these regimes the figures also show the projected data if PWIA were valid. For both projections the same amount of beam time has been assumed. It is important to note that at the lowest Q^2 value of 0.8 (GeV/c)^2 the eikonal approach is not expected to be valid for neutron angles below 60° and missing momenta of 0.2 GeV/c, 0.4 GeV/c, and 0.5 GeV/c, since the proton momenta are still well below 1 GeV/c in these cases. This limit has been marked with a dashed vertical line on each relevant graph.

The measurements at p_{miss} =0.5 GeV/c are of a more exploratory nature. The effects due to FSI in perpendicular kinematics are predicted to be even larger than for 0.4 GeV/c. Due to the reduced cross section we will therefore measure these points with a statistical precision of 7.5 %. This will reduce the necessary beam time considerably while still providing an excellent measurement.

p_{miss} GeV/c	θ_{nq} deg	e' MeV	θ_e deg	p MeV/c	θ_p deg
0^{ab}		1920.0	24.29	993.0	−52.78
0.10^{b}	84	1920.0	24.29	986.0	−58.57
0.10^{a}	84	1920.0	24.29	986.0	−47.00
0.20	20	2060.5	23.45	755.3	−65.92
0.20	40	2026.7	23.65	808.2	−67.89
0.20	60	1973.5	23.97	887.5	−66.96
0.20	70	1940.9	24.17	934.2	−65.52
0.20^{b}	76	1920.0	24.29	964.0	−64.40
0.20^{a}	76	1920.0	24.29	964.0	−41.16
0.20	90	1867.4	24.65	1035.8	−61.17
0.20	110	1788.5	25.20	1140.1	−55.63
0.20	150	1652.7	26.23	1311.1	−44.48
0.30^{b}	69	1920.0	24.29	928.0	−70.35
0.30^{a}	69	1920.0	24.29	928.0	−35.21
0.40	20	2107.9	23.18	567.5	−77.53
0.40	40	2039.8	23.57	690.0	−81.38
0.40^{b}	62	1920.0	24.29	877.0	−76.48
0.40^{a}	62	1920.0	24.29	877.0	−29.08
0.40	70	1863.3	24.68	958.2	−72.92
0.40	80	1786.2	25.22	1063.5	−67.78
0.40	90	1700.3	25.86	1175.6	−62.02
0.40	110	1503.1	27.53	1419.3	−49.69
0.50	20	2103.3	23.21	488.9	−83.77
0.50	40	2016.6	23.71	655.7	−87.51
0.50^{b}	55	1920.0	24.29	813.0	−82.91
0.50	70	1788.6	25.20	1002.0	−74.11
0.50	90	1566.0	26.96	1290.2	−59.45

Table 2: Kinematics for E_{inc} = 2.35 GeV/c and Q^2 =0.8 (GeV/c)^2. The superscripts (a,b) indicate the kinematics used for the R_{LT} separation (except the p_{miss} =0.50 GeV/c point where only the cross section on one side of $\vec{q}$ will me measured) in proposal PR-01-007. These kinematics must be done in one sequence, since the electron kinematics are fixed for these measurements.

p_{miss} GeV/c	θ_{nq} deg	e' MeV	θ_e deg	p MeV/c	θ_p deg
0^{ab}		3576.0	20.36	1834.0	−42.72
0.10^{+}	0	3745.0	19.89	1635.0	−47.25
0.10^{b}	85	3576.0	20.36	1828.0	−45.84
0.10^{a}	85	3576.0	20.36	1828.0	−39.59
0.10^{-}	180	3346.0	21.06	2083.0	−37.31
0.20^{+}	0	3872.0	19.56	1469.0	−50.95
0.20	40	3793.2	19.76	1561.5	−53.34
0.20	60	3699.5	20.01	1670.0	−51.92
0.20	70	3641.2	20.17	1736.5	−50.62
0.20^{b}	80	3576.0	20.36	1810.0	−48.97
0.20^{a}	80	3576.0	20.36	1810.0	−36.47
0.20	90	3507.0	20.56	1887.7	−47.09
0.20	110	3359.4	21.01	2051.1	−42.86
0.20	150	3098.1	21.89	2335.4	−34.78
0.20^{-}	180	3022.0	22.17	2417.0	−30.96
0.30^{+}	0	3966.0	19.32	1324.0	−53.90
0.30^{b}	75	3576.0	20.36	1781.0	−52.09
0.30^{a}	75	3576.0	20.36	1781.0	−33.35
0.30^{-}	180	2541.0	24.20	2900.0	−23.62
0.35^{-}	180	2200.0	26.05	3240.0	−19.53
0.40^{+}	0	4036.0	19.15	1194.0	−56.17
0.40	40	3885.7	19.52	1380.0	−62.11
0.40	60	3701.5	20.01	1597.8	−58.55
0.40^{b}	71	3576.0	20.36	1742.0	−55.22
0.40^{a}	71	3576.0	20.36	1742.0	−30.22
0.40	80	3445.4	20.75	1888.9	−51.59
0.40	90	3289.6	21.24	2061.4	−47.29
0.40	110	2922.3	22.55	2459.2	−38.04
0.50^{+}	0	4085.0	19.04	1074.0	−57.82
0.50	40	3896.9	19.49	1313.7	−65.88
0.50^{b}	66	3576.0	20.36	1693.0	−58.36
0.50^{a}	66	3576.0	20.36	1693.0	−27.07
0.50	90	3114.8	21.83	2205.2	−45.74

Table 3: Kinematics for E_{inc} = 4.7 GeV/c and Q^2 =2.10 (GeV/c)^2. The superscripts (a,b) indicate the kinematics used for the R_{LT} separation in proposal PR-01-007. These kinematics must be done in one sequence, since the electron kinematics are fixed for these measurements. The superscripts (+,−) indicate the kinematics used for the parallel/anti-parallel kinematics in proposal PR-01-007.

p_{miss} GeV/c	θ_{nq} deg	e' MeV	θ_e deg	p MeV/c	θ_p deg
0^{ab}		2828.0	29.74	2647.0	−32.01
0.10^{b}	86	2828.0	29.74	2641.0	−34.17
0.10^{a}	86	2828.0	29.74	2641.0	−29.85
0.20	20	3230.6	27.78	2192.0	−41.06
0.20	40	3148.9	28.15	2280.6	−40.91
0.20	60	3017.0	28.77	2422.6	−39.34
0.20	70	2934.3	29.18	2511.1	−38.08
0.20^{b}	81	2828.0	29.74	2624.0	−36.33
0.20^{a}	81	2828.0	29.74	2624.0	−27.69
0.20	90	2742.0	30.21	2715.5	−34.85
0.20	110	2527.7	31.49	2941.3	−31.09
0.20	150	2142.1	34.29	3343.8	−24.10
0.30^{b}	77	2828.0	29.74	2597.0	−38.48
0.30^{a}	77	2828.0	29.74	2597.0	−25.54
0.40	20	3458.1	26.83	1874.6	−48.22
0.40	40	3306.8	27.45	2042.4	−48.04
0.40	60	3053.6	28.59	2318.1	−44.49
0.40^{b}	73	2828.0	29.74	2560.0	−40.61
0.40^{a}	73	2828.0	29.74	2560.0	−23.41
0.40	80	2693.3	30.49	2702.9	−38.25
0.40	90	2470.3	31.87	2937.9	−34.45
0.40	110	1935.9	36.13	3494.8	−26.17
0.50	20	3529.9	26.55	1745.2	−51.28
0.50	40	3343.1	27.30	1954.7	−51.03
0.50	70	2812.2	29.82	2530.8	−42.44
0.50	90	2251.9	33.42	3121.4	−32.96

Table 4: Kinematics for E_{inc} = 4.7 GeV/c and Q^2 =3.50 (GeV/c)^2. The superscripts (a,b) indicate the kinematics used for the R_{LT} separation in proposal PR-01-007. These kinematics must be done in one sequence, since the electron kinematics are fixed for these measurements.

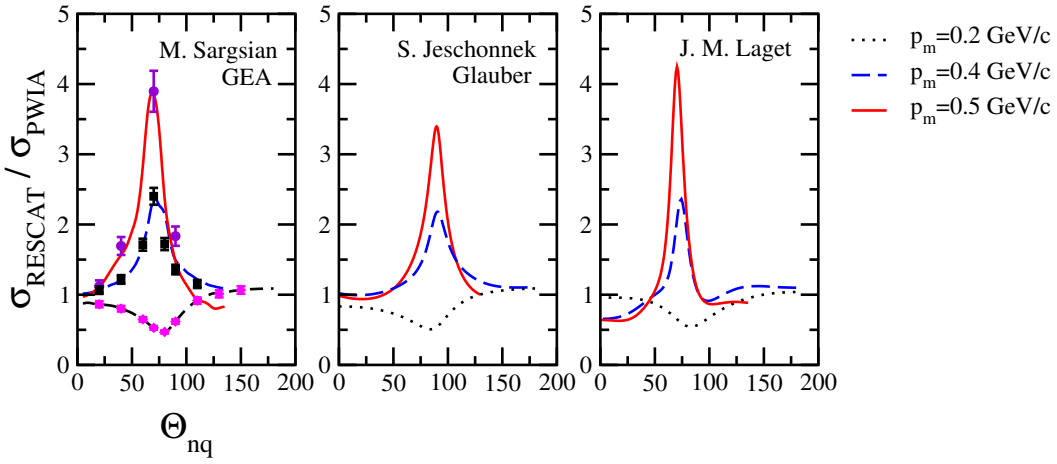

Figure 21: The ratio between the ^{2}H$(e,e'p)$ cross section calculated including FSI and PWIA for Q^2 =4 (GeV/c)^2. The Calculations are by S. Jeschonnek, J.M. Laget, and M. Sargsian. The points with error bars indicate the projected experimental data.

This experiment will use the standard Hall A setup, including the high resolution spectrometer pair. The 6 msr collimators would be used for both spectrometers. The standard detection systems including scintillator stack, VDCs and Particle ID counters (Aerogel Čerenkov in the proton arm and gas Čerenkov + shower counter in the electron arm) would be needed. The PID requirements of this experiment are quite modest.

Targets include the 15 cm liquid deuterium cryogenic target, the 15 cm liquid hydrogen target for calibration of the cross section and for kinematic definition and a thin carbon foil for spectrometer pointing studies.

Unpolarized beam of 100 μA maximum current is needed along with the standard beam rastering and monitoring equipment. The entire experiment would be run at beam energies of 2.35 and 4.7 GeV.

Single-arm background rates for (e,e') were calculated with the computer code QFSV and for (e,p), (e,π^+) and (e,π^-) with the electro-production code EPC, both of Lightbody and O'Connell [62]. These codes were embedded in the $(e,e'p)$ Monte Carlo code, MCEEP [63], allowing the single-arm cross sections to be folded with the acceptance of the respective spectrometer. The results are shown in Tables 5, 6 and 7. The beam current was selected to keep the single-arm rates below 500 kHz per arm. The rates are not atypical of Hall A experiments and should pose no problems.

The coincidence rates were calculated with the $(e,e'p)$ Monte Carlo code, MCEEP [63] using the PWBA model of Jeschonnek and the Argonne V18 wave function radiatively folded within MCEEP. This code has been used extensively to model experiments and compare data to folded theoretical calculations. The rates are given in Tables 8, 9 and 10.

The coincidence rates and counting times are based on the following:

- **DAQ Rate:** Beam current ($\leq$ 100 μA) was chosen so that DAQ Rate $\leq$ 2 kHz. This is the total data acquisition rate which includes real coincidences and accidental coincidences within an 80 ns timing gate. The accidentals rates are based on products of the singles rates in each arm and include contributions from (e,e') and (e,π^-) in the electron arm and from (e,p) and (e,π^+) in the proton arm.

p_{miss} GeV/c	θ_{nq} deg	Beam Current μA	(e,e') kHz	(e,π^-) kHz	(e,p) kHz	(e,π^+) kHz
0^{ab}		35	32	5	16	10
0.10^{b}	84	100	87	13	2	24
0.10^{a}	84	90	90	13	136	30
0.20	20	100	40	0	12	27
0.20	40	100	69	1	6	25
0.20	60	100	94	6	3	20
0.20	70	100	92	11	2	14
0.20^{b}	76	100	83	12	1	9
0.20^{a}	76	90	97	14	180	35
0.20	90	100	78	22	1	6
0.20	110	100	39	34	1	7
0.20	150	100	58	43	44	30
0.30^{b}	69	100	79	11	1	0
0.30^{a}	69	75	88	13	195	33
0.40	20	100	6	0	53	24
0.40	40	100	56	1	8	20
0.40^{b}	62	100	77	11	1	0
0.40^{a}	62	30	38	5	100	15
0.40	70	100	72	21	1	0
0.40	80	100	35	31	1	0
0.40	90	100	41	35	1	0
0.40	110	100	36	41	1	0
0.50	20	100	8	0	76	23
0.50	40	100	73	2	7	15
0.50^{b}	55	100	76	11	1	0
0.50	70	100	35	30	1	0
0.50	90	100	44	36	1	0

Table 5: Singles rates for E_{inc} = 2.35 GeV/c and Q^2 =0.8 (GeV/c)^2. The superscripts (a,b) indicate the kinematics used for the R_{LT} separation (except the p_{miss} =0.50 GeV/c point where only the cross section on one side of $\vec{q}$ will me measured) in proposal PR-01-007.

p_{miss} GeV/c	θ_{nq} deg	Beam Current μA	(e,e') kHz	(e,π^-) kHz	(e,p) kHz	(e,π^+) kHz
0^{ab}		100	10	30	105	61
0.10^+	0	100	7	8	30	55
0.10^b	85	100	9	28	1	35
0.10^a	85	100	10	31	260	66
0.10^-	180	100	11	66	241	68
0.20^+	0	100	3	1	8	51
0.20	40	100	6	5	1	21
0.20	60	100	8	14	1	8
0.20	70	100	9	21	1	5
0.20^b	80	100	9	27	1	4
0.20^a	80	100	11	32	294	70
0.20	90	100	11	43	1	7
0.20	110	100	12	68	1	17
0.20	150	100	15	89	229	74
0.20^-	180	70	10	57	215	53
0.30^+	0	100	1	0	5	48
0.30^b	75	100	9	26	1	0
0.30^a	75	100	11	34	323	73
0.30^-	180	70	11	59	243	60
0.35^-	180	70	8	59	256	62
0.40^+	0	100	0	0	10	46
0.40	40	100	3	1	1	0
0.40	60	100	7	13	1	0
0.40^b	71	100	8	25	1	0
0.40^a	71	100	11	35	352	77
0.40	80	100	11	50	1	0
0.40	90	100	11	71	1	0
0.40	110	100	16	86	1	1
0.50^+	0	100	0	0	33	44
0.50	40	100	3	1	1	0
0.50^b	66	100	8	24	0	0
0.50^a	66	30	4	11	115	24
0.50	90	100	13	77	1	0

Table 6: Singles rates for E_{inc} = 4.7 GeV/c and Q^2 =2.10 (GeV/c)^2. The superscripts (a,b) indicate the kinematics used for the R_{LT} separation in proposal PR-01-007. The superscripts (+,−) indicate the kinematics used for the parallel/anti-parallel kinematics in proposal PR-01-007.

p_{miss} GeV/c	θ_{nq} deg	Beam Current μA	(e,e') kHz	(e,π^-) kHz	(e,p) kHz	(e,π^+) kHz
0^{ab}		100	1	30	114	33
0.10^{b}	86	100	1	29	9	5
0.10^{a}	86	100	1	31	269	67
0.20	20	100	0	0	1	8
0.20	40	100	0	2	1	1
0.20	60	100	0	9	1	0
0.20	70	100	0	18	1	0
0.20^{b}	81	100	0	29	0	0
0.20^{a}	81	100	1	31	306	75
0.20	90	100	1	47	1	0
0.20	110	100	1	73	7	1
0.20	150	100	1	81	181	19
0.30^{b}	77	100	0	28	0	0
0.30^{a}	77	100	1	32	324	78
0.40	20	100	0	0	1	2
0.40	40	100	0	0	1	0
0.40	60	100	0	5	0	0
0.40^{b}	73	100	0	27	0	0
0.40^{a}	73	100	1	33	340	81
0.40	80	100	1	52	0	0
0.40	90	100	1	74	0	0
0.40	110	100	1	77	1	0
0.50	20	100	0	0	1	1
0.50	40	100	0	0	1	0
0.50	70	100	1	33	0	0
0.50	90	100	1	76	0	0

Table 7: Singles rates for E_{inc} = 4.7 GeV/c and Q^2 =3.50 (GeV/c)^2. The superscripts (a,b) indicate the kinematics used for the R_{LT} separation in proposal PR-01-007.

p_{miss} GeV/c	θ_{nq} deg	Coin Rate hr^{-1} (per bin)	Time hours	Error %
0^{ab}		912000	8.4E-03	1.4
0.10^{b}	84	321000	1.76E-02	1.6
0.10^{a}	84	211000	2.88E-02	1.6
0.20	20	13000	2.48E-02	5.6
0.20	40	17100	1.84E-02	5.6
0.20	60	21300	1.52E-02	5.6
0.20	70	25400	1.20E-02	5.6
0.20^{b}	76	22500	2.32E-01	1.6
0.20^{a}	76	9600	7.12E-01	1.6
0.20	90	27200	1.20E-02	5.6
0.20	110	27200	1.20E-02	5.6
0.20	150	22600	1.44E-02	5.6
0.30^{b}	69	3310	1.60E+00	1.6
0.30^{a}	69	768	6.96E+00	2.3
0.40	20	440	7.20E-01	5.6
0.40	40	950	3.36E-01	5.6
0.40^{b}	62	1010	5.20E+00	1.6
0.40^{a}	62	77	1.76E+01	5.6
0.40	70	1770	1.84E-01	5.6
0.40	80	1720	1.84E-01	5.6
0.40	90	1750	1.84E-01	5.6
0.40	110	1670	1.92E-01	5.6
0.50	20	130	9.60E-01	8.4
0.50	40	420	3.44E-01	8.4
0.50^{b}	55	441	5.36E+00	2.3
0.50	70	870	1.60E-01	8.4
0.50	90	790	1.84E-01	8.4

Table 8: Coincidence rates for E_{inc} = 2.35 GeV/c and Q^2 =0.8 $(GeV/c)^2$. The superscripts (a,b) indicate the kinematics used for the R_{LT} separation (except the p_{miss} =0.50 GeV/c point where only the cross section on one side of $\vec{q}$ will me measured) in proposal PR-01-007. The rates are average per hour into each bin, where a bin is defined by Δp_{miss} = $\pm$20 MeV/c and $\Delta\theta_{nq}$ = $\pm 5^{\circ}$, except for the (a,b) points where a bin is defined by Δp_{miss} = $\pm$20 MeV/c only. All rates include estimates for radiative effects. The times are for the indicated error per bin.

p_{miss} GeV/c	θ_{nq} deg	Coin Rate hr^{-1} (per bin)	Time hours	Error %
0^{ab}		274000	2.60E-02	1.4
0.10^{+}	0	134000	4.08E-02	1.6
0.10^{b}	85	81600	6.72E-02	1.6
0.10^{a}	85	67200	8.80E-02	1.6
0.10^{-}	180	67200	8.80E-02	1.6
0.20^{+}	0	12500	4.24E-01	1.6
0.20	40	1190	2.72E-01	5.6
0.20	60	1220	2.64E-01	5.6
0.20	70	1220	2.64E-01	5.6
0.20^{b}	80	7200	7.36E-01	1.6
0.20^{a}	80	4220	1.44E+00	1.6
0.20	90	1590	2.00E-01	5.6
0.20	110	2080	1.52E-01	5.6
0.20	150	1970	1.60E-01	5.6
0.20^{-}	180	2450	2.48E+00	1.6
0.30^{+}	0	1010	2.24E+00	2.3
0.30^{b}	75	1100	4.72E+00	1.6
0.30^{a}	75	408	8.80E+00	2.3
0.30^{-}	180	202	7.28E+00	3.9
0.35^{-}	180	62	8.80E+00	7.8
0.40^{+}	0	149	5.60E+00	5.6
0.40	40	180	1.76E+00	5.6
0.40	60	340	9.60E-01	5.6
0.40^{b}	71	336	6.88E+00	2.3
0.40^{a}	71	82	1.92E+01	5.6
0.40	80	330	9.60E-01	5.6
0.40	90	290	1.12E+00	5.6
0.40	110	230	1.36E+00	5.6
0.50^{+}	0	43	9.60E+00	5.0
0.50	40	140	1.04E+00	8.4
0.50^{b}	66	158	5.20E+00	3.9
0.50^{a}	66	8	3.52E+01	11.9
0.50	90	220	6.72E-01	8.4

Table 9: Coincidence rates for E_{inc} = 4.7 GeV/c and Q^2 =2.10 (GeV/c)^2. The superscripts (a,b) indicate the kinematics used for the R_{LT} separation in proposal PR-01-007. The superscripts (+,−) indicate the kinematics used for the parallel/anti-parallel kinematics in proposal PR-01-007. The rates are average per hour into each bin, where a bin is defined by Δp_{miss} = ±20 MeV/c and $\Delta\theta_{nq}$ = ±5°, except for the (a,b) and (+,−) points where a bin is defined by Δp_{miss} = ±20 MeV/c only. All rates include estimates for radiative effects. The times are for the indicated error per bin.

p_{miss} GeV/c	θ_{nq} deg	Coin Rate hr^{-1} (per bin)	Time hours	Error %
0^{ab}		35000	1.90E-01	1.4
0.10^{b}	86	17300	3.04E-01	1.6
0.10^{a}	86	15800	3.60E-01	1.6
0.20	20	150	2.16E+00	5.6
0.20	40	200	1.60E+00	5.6
0.20	60	160	2.00E+00	5.6
0.20	70	150	2.24E+00	5.6
0.20^{b}	81	1970	2.64E+00	1.6
0.20^{a}	81	1060	5.52E+00	1.6
0.20	90	170	1.92E+00	5.6
0.20	110	220	1.44E+00	5.6
0.20	150	150	2.24E+00	5.6
0.30^{b}	77	221	1.04E+01	2.3
0.30^{a}	77	82	1.28E+01	3.9
0.40	20	15	2.13E+01	5.6
0.40	40	25	1.34E+01	5.6
0.40	60	38	8.69E+00	5.6
0.40^{b}	73	47	8.69E+00	5.6
0.40^{a}	73	13	5.61E+01	5.6
0.40	80	35	8.69E+00	5.6
0.40	90	23	1.34E+01	5.6
0.40	110	12	2.53E+01	5.6
0.50	20	8	1.56E+01	8.4
0.50	40	15	7.80E+00	8.4
0.50	70	46	3.12E+00	8.4
0.50	90	15	1.09E+01	8.4

Table 10: Coincidence rates for E_{inc} = 4.7 GeV/c and Q^2 =3.50 (GeV/c)^2. The superscripts (a,b) indicate the kinematics used for the R_{LT} separation in proposal PR-01-007. The rates are average per hour into each bin, where a bin is defined by Δp_{miss} = $\pm$20 MeV/c and $\Delta\theta_{nq}$ = $\pm5^{\circ}$, except for the (a,b) points where a bin is defined by Δp_{miss} = $\pm$20 MeV/c only. All rates include estimates for radiative effects. The times are for the indicated error per bin.

- **Singles Rates:** The singles rates in each arm were always kept below 500 kHz.

- **Coin Rate:** This is the real coincidence rate, including radiative effects, per hour and into each kinematic bin. A bin is defined by $\Delta p_{miss} = \pm 20$ MeV/c and $\Delta\theta_{nq} = \pm 5^{\circ}$, except for the (a,b) and $(+,-)$ points where a bin is defined by $\Delta p_{miss} = \pm 20$ MeV/c only. The radiative tail was cut on missing mass ($\epsilon_m < 10$ MeV; about 8 MeV above the breakup threshold). This cut is necessary, since, otherwise, radiative effects can cause substantial feeding from low recoil momentum to high, heavily biasing the spectrum.

- **S:N:** The signal-to-noise ratio ≥ 0.5. This is the reals rate divided by the accidentals rate into a 5 ns timing window. Here, the accidentals rates include only (e, e') in the electron arm and (e, p) in the proton arm since particle ID will almost completely remove the other backgrounds. Further, it's assumed that accidentals are reduced by a factor of 5 from requiring a consistent vertex from both spectrometers and another factor of 10 from a missing mass cut.

- **Time:** The acquisition times are for the quoted statistical errors. They include computer deadtime of 10% per kHz data acquisition rate as well as an overall 30% inefficiency factor. This 30% inefficiency is based on experience from Experiment E94-004 and reflects anticipated acceptance cuts to eliminate the relatively poorly understood edges as well as VDC hit multiplicity cuts to deal with multiple track events (especially important at the higher singles rates). (The radiative losses have already been included in the coincidence rates.)

- **Err:** The statistical uncertainty per 40 MeV/c bin in p_r. Each measurement comprises roughly 7.5 of these bins. The statistical uncertainty includes contributions from the accidentals within the coincidence resolving time (assumed here to be 5 ns).

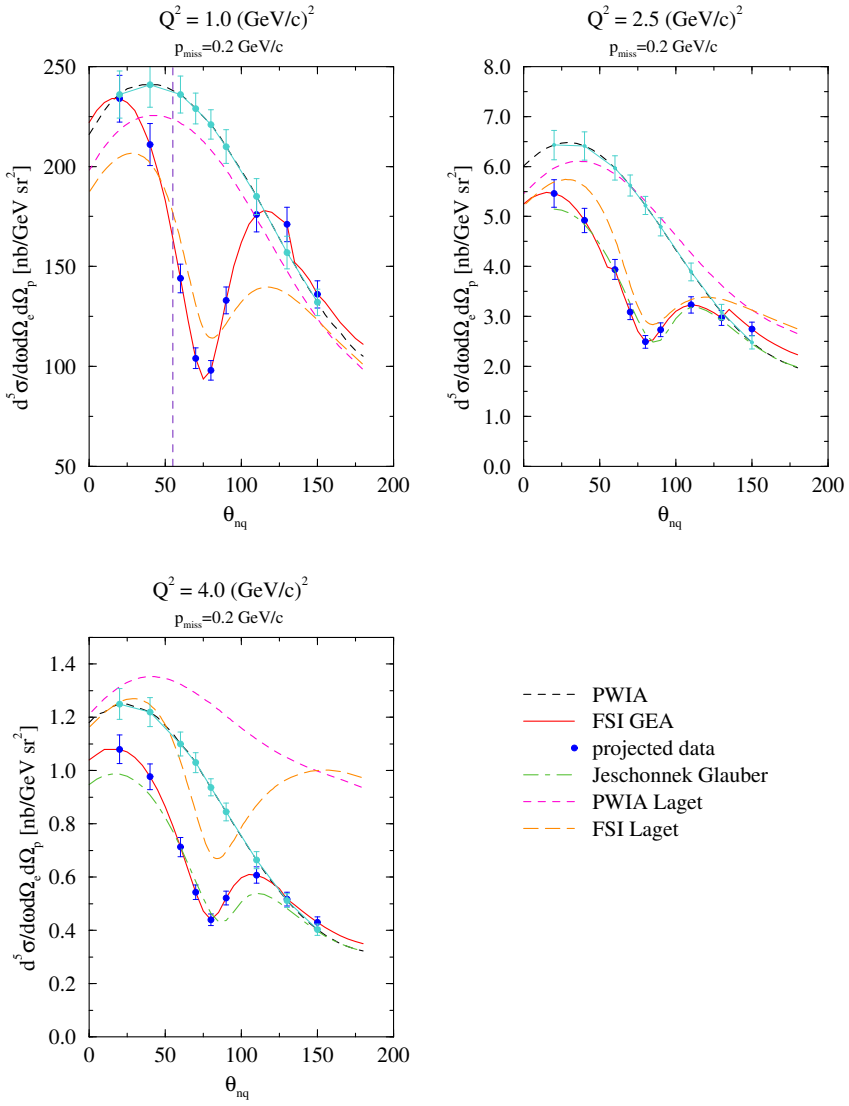

Figure 22: The ^{2}H$(e,e'p)$ cross section for p_{miss} =0.2 GeV/c as a function of the recoil angle (θ_{nq}) and for various Q^2 values. Note that for small neutron angles and at Q^2 = 1.0 (GeV/c)^2 the eikonal approximation breaks down (curves left of the dashed vertical line illustrate this point).

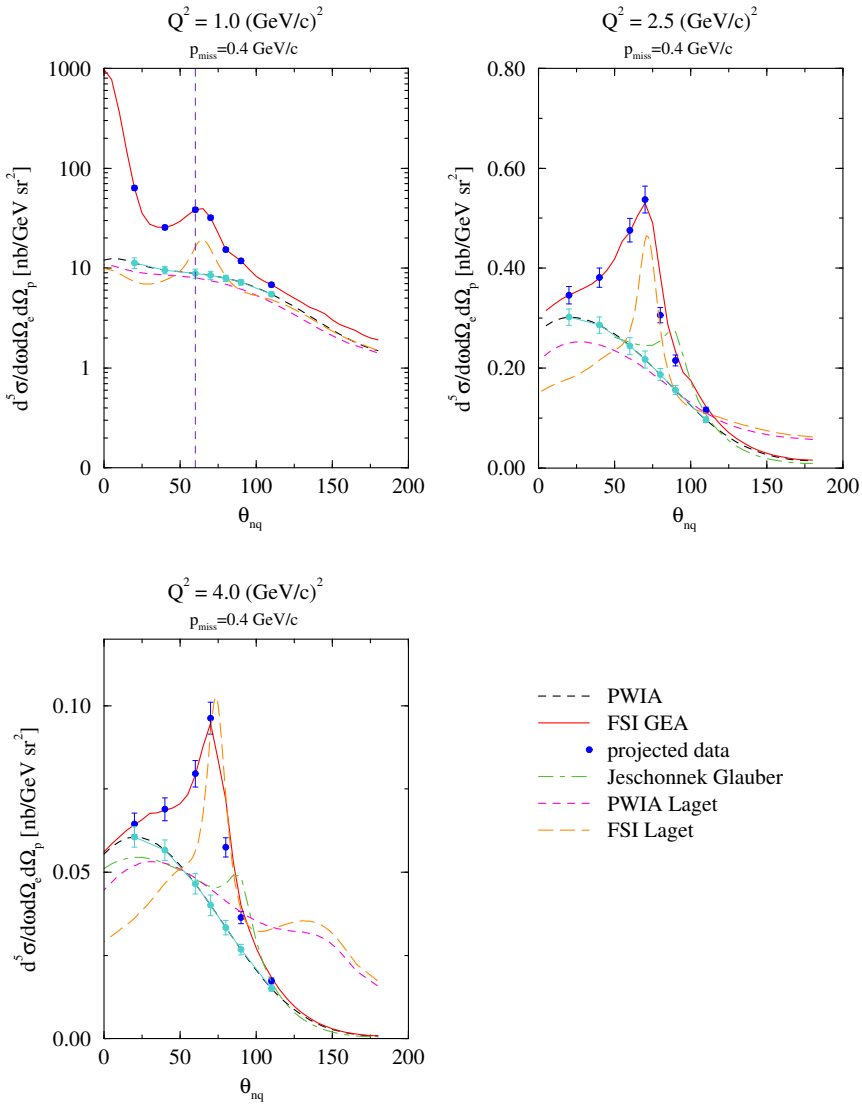

Figure 23: The ^{2}H$(e,e'p)$ cross section for p_{miss} =0.4 GeV/c as a function of the recoil angle (θ_{nq}) and for various Q^2 values. Note that for small neutron angles and at Q^2 = 1.0 (GeV/c)^2 the eikonal approximation breaks down (curves left of the dashed vertical line illustrate this point).

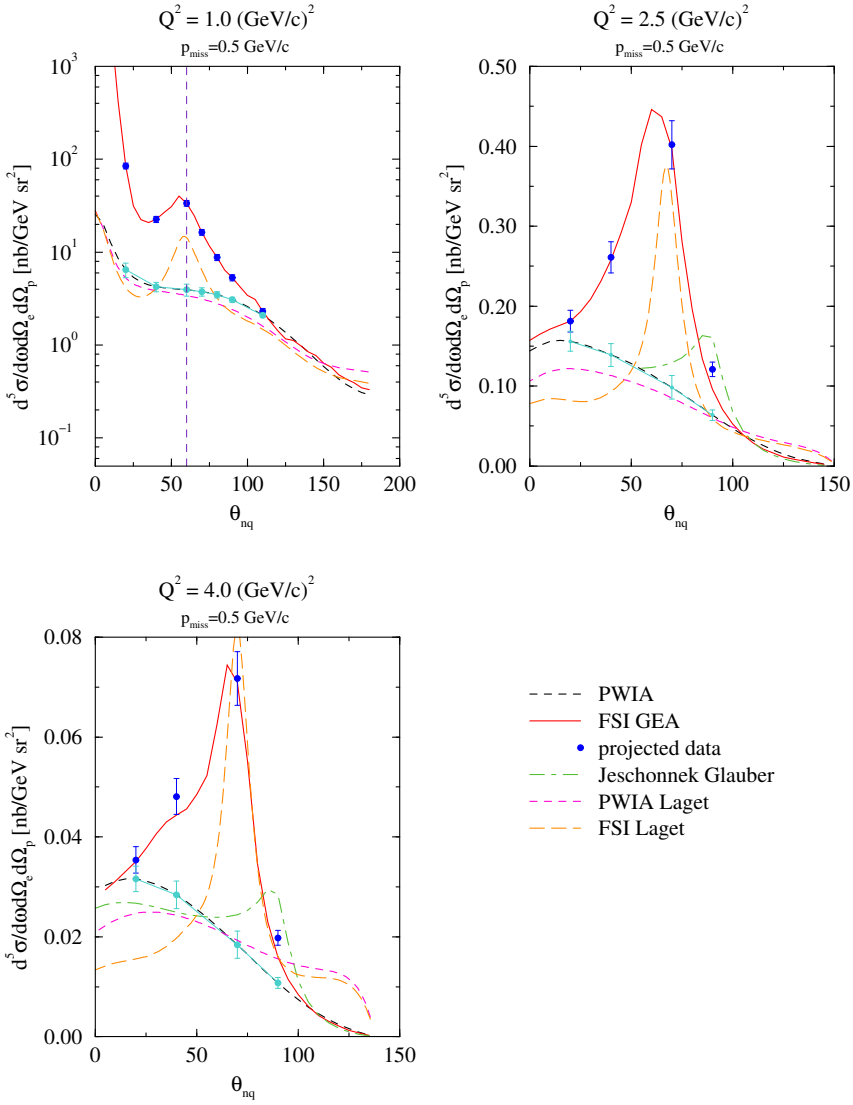

Figure 24: The ^{2}H$(e,e'p)$ cross section for p_{miss} =0.5 GeV/c as a function of the recoil angle (θ_{nq}) and for various Q^2 values. Note that for small neutron angles and at Q^2 = 1.0 (GeV/c)^2 the eikonal approximation breaks down (curves left of the dashed vertical line illustrate this point).

5 Beam Time Summary

Table 11 shows the summary of the requested beam time. Acquisition time is assumed to be 0.5 hours minimum per point for the high rate measurements. The beam time on target required to achieve the necessary statistics includes the following items (the first two are included as "Overhead" items per kinematic point):

- Time to check the spectrometer pointing (0.5 hr/setting).
- Time for field and angle changes (2.0 hr/setting).
- Time for target changes.
- Measurements on the dummy target cell.
- 1 hour for elastic scattering at each value of Q^2.

Q^2 (GeV/c)^2	p_{miss} (GeV/c)	Data Taking	Overhead	Subtotal
0.8	0	0.5	2.5	3.0
	0.10	1.0	5.0	6.0
	0.20	4.6	22.5	27.1
	0.30	8.6	5.0	13.6
	0.40	26.0	20.0	46.0
	0.50	7.8	12.5	20.3
TOTAL Q1				116.0
2.1	0	0.5	2.5	3.0
	0.10	2.0	10.0	12.0
	0.20	8.2	25.0	33.2
	0.30	23.0	10.0	33.0
	0.35	8.8	2.5	11.3
	0.40	37.8	20.0	57.8
	0.50	51.7	12.5	64.2
TOTAL Q2				214.5
3.5	0	0.5	2.5	3.0
	0.10	1.0	5.0	6.0
	0.20	21.8	22.5	44.3
	0.30	23.2	5.0	28.2
	0.40	155.6	20.0	175.6
	0.50	37.4	10.0	47.4
TOTAL Q3				304.5
Elastic Calibrations				3.0
Optics Commissioning				24.0
Target Commissioning				16.0
Dummy Cell Measurements				12.0
BCM Calibrations				8.0
Arc+ep Energy Measurements				8.0
Harp Scans				8.0
White Spectrum Scans				6.0
TOTAL COMMISSIONING				85.0
GRAND TOTAL				720.0

Table 11: Beam time overview (all times in hours).

References

[1] C. Marchand *et al.*, Phys. Rev. Lett. **60**, 1703 (1988).

[2] JLAB Hall A Experiment E00-102, *Testing the Limits of the Single Particle Model in* $^{16}O(e,e'p)$*: An Update to E89-003*, W. Bertozzi, K. Fissum, A. Saha and L. Weinstein, co-spokespersons.

[3] J. Gao *et al.*, Phys. Rev. Lett. **84**, 3265 (2000).

[4] W. Fabian and H. Arenhövel, Nucl. Phys. **A314**, 253 (1979).

[5] M. van der Schaar *et al.*, Phys. Rev. Lett. **68**, 776 (1992).

[6] E. Hummel and J.A. Tjon, Phys. Rev. C**49**, 21 (1994).

[7] R.G. Arnold, C.E. Carlson and F. Gross, Phys. Rev. C **23**, 363 (1981); H. Arenhövel, W. Leidemann and E.L. Tomusiak, Z. Phys. A **331**, 123 (1988).

[8] H. Arenhövel, Phys. Lett. **B199**, 13 (1987) and private communication; A.Yu. Korchin, Yu.P. Mel'nik and A.V. Shebeko, Sov. J. Nucl. Phys. **48**, 243 (1988); M.P. Rekalo, G.I. Gakh and A.P. Rekalo, J. Phys. G. **15**, 1223 (1989).

[9] M. Bernheim *et al.*, Nucl. Phys. **A365**, 349 (1981).

[10] S. Turck-Chieze *et al.*, Phys. Lett. **142B**, 145 (1984).

[11] H. Breuker *et al.*, Nucl. Phys. **A455**, 641 (1986).

[12] K.I. Blomqvist *et al.*, Phys. Lett. B **424**, 33 (1998).

[13] T. Tamae *et al.*, Phys. Rev. Lett. **59**, 2919 (1987).

[14] M. van der Schaar *et al.*, Phys. Rev. Lett. **66**,2855 (1991).

[15] F. Frommberger *et al.*, Phys. Lett. B **339**, 17 (1994).

[16] J.E. Ducret *et al.*, Phys. Rev. C **49**, 1783 (1994).

[17] H.J. Bulten *et al.*, Phys. Rev. Lett. **74**, 4775 (1995).

[18] D. Jordan *et al.*, Phys. Rev. Lett. **76**, 1579 (1996).

[19] A. Pellegrino *et al.*, Phys. Rev. Lett. **78**, 4011 (1997).

[20] W.-J. Kasdorp *et al.*, Phys. Lett. B **393**, 42 (1997).

[21] B.D. Milbrath *et al.*, Phys. Rev. Lett. **80**, 452 (1998).

[22] B.D. Barkhuff, Ph.D. thesis, MIT (1997).

[23] K. Joo, Ph.D. thesis, MIT (1997).

[24] H. Arenhövel, private communication (2000).

[25] J.W. Van Orden, N. Devine and F. Gross, Phys. Rev. Lett. **75**, 4369 (1995).

[26] S. Jeschonnek and T.W. Donnelly, Phys. Rev. C **57**, 2438 (1998).

[27] S. Jeschonnek and J.W. Van Orden, Phys. Rev. C **62**, 044613 (2000).

[28] L.C. Alexa *et al.*, Phys. Rev. Lett. **82** (1999) 1374.

[29] W. Van Orden, *The Deuteron in the Light of the New Data from JLab*, Plenary talk at the Jefferson Lab User Meeting, 24-25 June 1999.

[30] S. Rock *et al.*, Phys. Rev. **D46** (1992) 24; P. Bosted, R.G. Arnold, S. Rock and Z.M. Szalata, Phys. Rev. Lett. **49** (1982) 1380.

[31] O. Benhar, A. Fabrocini, S. Fantoni, G.A. Miller, V.R. Pandharipande, and I. Sick, Phys. Rev. **C44** (1991) 2328.

[32] O. Benhar, A. Fabrocini, S. Fantoni, V.R. Pandharipande, and I. Sick, Phys. Rev. **C5** (1994).

[33] L.L. Frankfurt, M.I. Strikman, D.B. Day and M.M. Sargsian, Phys. Rev. **C48** (1993) 2451.

[34] A. Bussiere *et al.*, Nucl. Phys. **A365** (1981) 349. %

[35] K.I. Blomqvist *et al.*, Phys. Lett.**B424** (1998) 33.

[36] R.J. Glauber, Phys. Rev. **100** (1955) 242.

[37] L.L. Frankfurt, W.G. Greenberg, J.A. Miller, M.M. Sargsian and M.I. Strikman, Z. Phys. **A352** (1995) 97.

[38] L.L. Frankfurt, M.M. Sargsian and M.I. Strikman, Phys. Rev. **C56** (1997) 1124.

[39] T.G. O'Neill *et al.*, Phys. Lett. **B351** (1995) 87.

[40] D. Abbott *et al.*, Phys. Rev. Lett. **80** (1998) 5072.

[41] H. Arenhovel, W. Leidemann and E.L. Tomusiak, Phys. ReV. **C46** (1992) 455.

[42] J.-M. Laget, in *Modern Topics in Electron Scattering*, Ed. by B. Frois and I. Sick (World Scientific, 1991) 290, and references therein.

[43] J.-M. Laget, Nucl. Phys. **A579** (1994) 333.

[44] E. Voutier, V. Breton, J.-M. Laget, C. Marchand, J. Marroncle, J.-F. Mathiot, A. Pastor and Th. Russew, Proceedings of the ELFE Workshop on Hadronic Physics, Ed. by N. d'Hose *et al.* (St-Malo, 1996) 107;
J.-M. Laget, Proceedings of the Workshop on Color Transparency (http://isnwww.in2p3.fr/ct97), Ed. E. Voutier (Grenoble, 1997) 131.

[45] J.-M. Laget, Physics and Instrumentation with 6-12 GeV Beams, Ed. by S. Dytman *et al.* (Newport News, 1998), p.57.

[46] A. Bianconi,S. Jeschonnek, N.N. Nikolaev and B.G. Zakharov, Phys. Lett. **B343** (1995) 13.

[47] S. Jeschonnek, **nucl-th/0009086** (2000).

[48] D.O. Riska, Phys. Rep. **181** (1989) 207.

[49] J. Speth and A.W. Thomas, Adv. Nucl. Phys.**24** (1997) 83.

[50] H. Arenhovel, in *Modern Topics in Electron Scattering*, Ed. by B. Frois and I. Sick (World Scientific, 1991) 136.

[51] L.L. Frankfurt, G.A. Miller, M.M. Sargsian and M.I. Strikman, Phys. Rev. Lett. **84** (2000) 3045.

[52] L.L. Frankfurt and M.I. Strikman, Phys. Rep. **76**, (1981) 215; Phys. Rep. **160**, (1988).

[53] F. Gross, Phys. Rev. **C26** (1982) 2203.

[54] B.D. Keister and W.N. Polyzou, in *Advances in Nuclear Physics*, Ed. J.W. Negele and E. Voght, **V.20** (1991) 225.

[55] L.A. Kondratyuk, J. Vogelzang and M.S. Franchesko, Phys. Lett. **B98** (1981) 405.

[56] J. Carbonell, B. Desplanques, V.A. Karmanov and J.-F. Mathiot, Phys. Rep. **300** (1998) 215.

[57] T.J. de Forest, Nucl. Phys. **A392** (1983) 232.

[58] J.J. Aubert *et al.*, Phys. Lett. **B123** (1983) 275;
A. Bodek *et al.*, Phys. Rev. Lett. **50** (1983) 1431; Phys. Rev. Lett. **51** (1983) 534.

[59] L.L. Frankfurt and M.I. Strikman, Nucl. Phys. **B250** (1985) 143.

[60] M.R. Frank, B.K. Jennings, G.A. Miller, Phys.Rev **C54** (1996) 920.

[61] L.L. Frankfurt and M.I. Strikman, Phys. Rep. **160** (1988) 235.

[62] J.W. Lightbody and J.S. O'Connell, Computers in Physics, May/June 1988, p. 57.

[63] P.E. Ulmer, computer program MCEEP, *Monte Carlo for* $(e, e'p)$ *Experiments*, JLAB Technical Note # 91-101 (1991).